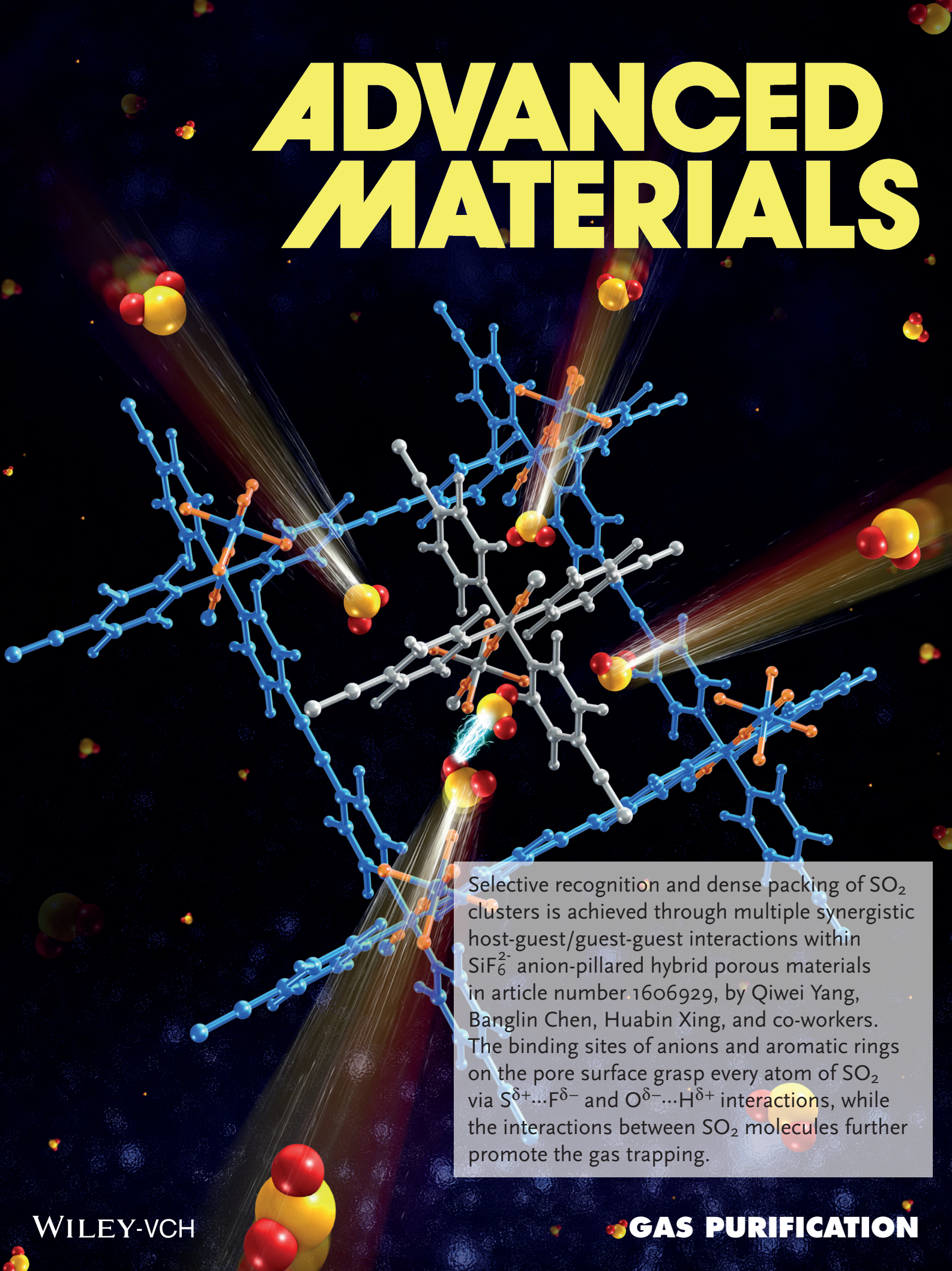


# ADVANCED MATERIALS



Selective recognition and dense packing of SO<sub>2</sub> clusters is achieved through multiple synergistic host-guest/guest-guest interactions within SiF<sub>6</sub><sup>2-</sup> anion-pillared hybrid porous materials in article number 1606929, by Qiwei Yang, Banglin Chen, Huabin Xing, and co-workers. The binding sites of anions and aromatic rings on the pore surface grasp every atom of SO<sub>2</sub> via S<sup>δ+</sup>...F<sup>δ-</sup> and O<sup>δ-</sup>...H<sup>δ+</sup> interactions, while the interactions between SO<sub>2</sub> molecules further promote the gas trapping.

# Ultrahigh and Selective SO<sub>2</sub> Uptake in Inorganic Anion-Pillared Hybrid Porous Materials

Xili Cui, Qiwei Yang,\* Lifeng Yang, Rajamani Krishna, Zhiguo Zhang, Zongbi Bao, Hui Wu, Qilong Ren, Wei Zhou, Banglin Chen,\* and Huabin Xing\*

The efficient capture of SO<sub>2</sub> is of great significance in gas-purification processes including flue-gas desulfurization and natural-gas purification, but the design of porous materials with high adsorption capacity and selectivity of SO<sub>2</sub> remains very challenging. Herein, the selective recognition and dense packing of SO<sub>2</sub> clusters through multiple synergistic host–guest and guest–guest interactions by controlling the pore chemistry and size in inorganic anion (SiF<sub>6</sub><sup>2-</sup>, SIFSIX) pillared metal–organic frameworks is reported. The binding sites of anions and aromatic rings in SIFSIX materials grasp every atom of SO<sub>2</sub> firmly via S<sup>δ+</sup>...F<sup>δ-</sup> electrostatic interactions and O<sup>δ-</sup>...H<sup>δ+</sup> dipole–dipole interactions, while the guest–guest interactions between SO<sub>2</sub> molecules further promote gas trapping within the pore space, which is elucidated by first-principles density functional theory calculations and powder X-ray diffraction experiments. These interactions afford new benchmarks for the highly efficient removal of SO<sub>2</sub> from other gases, even if at a very low SO<sub>2</sub> concentration. Exceptionally high SO<sub>2</sub> capacity of 11.01 mmol g<sup>-1</sup> is achieved at atmosphere pressure by SIFSIX-1-Cu, and unprecedented low-pressure SO<sub>2</sub> capacity is obtained in SIFSIX-2-Cu-i (4.16 mmol g<sup>-1</sup> SO<sub>2</sub> at 0.01 bar and 2.31 mmol g<sup>-1</sup> at 0.002 bar). More importantly, record SO<sub>2</sub>/CO<sub>2</sub> selectivity (86–89) and excellent SO<sub>2</sub>/N<sub>2</sub> selectivity (1285–3145) are also achieved. Experimental breakthrough curves further demonstrate the excellent performance of these hybrid porous materials in removing low-concentration SO<sub>2</sub>.

Rapid economic growth all over the world has resulted in the excessive energy consumption as well as increasing environmental burdens.<sup>[1,2]</sup> One of the most serious related problems is the emission of sulfur dioxide (SO<sub>2</sub>), induced by the utilization


of low-grade fossil fuels.<sup>[3–6]</sup> Besides the direct detriment on environment and human health, SO<sub>2</sub> will significantly inactivate the adsorbents or absorbents in removing CO<sub>2</sub> from flue gas although the concentration of SO<sub>2</sub> in flue gas is very low (cat. 2000 ppm).<sup>[7,8]</sup> Moreover, in the reactions such as selective catalytic reduction of NO<sub>x</sub> and catalytic combustion of CH<sub>4</sub>,<sup>[9,10]</sup> even trace amount of SO<sub>2</sub> could poison the catalysts and this deactivation is irreversible. The traditional flue-gas desulfurization (FGD) processes, with limestone or organic solvents as the absorbents,<sup>[11,12]</sup> can remove about 90–95% SO<sub>2</sub>. However, these FGD technologies are energy-intensive and not efficient for the deep desulfurization. Therefore, there is an urgent demand for efficient technology to remove trace SO<sub>2</sub> in flue gas and other SO<sub>2</sub>-containing gases.

In the past decades, the development of energy-efficient physical-adsorption separation technology shows great potential in gas separation, which greatly motivates the design and synthesis of highly efficient porous materials.<sup>[13–15]</sup> Metal–organic frameworks (MOFs) and/or porous coordination polymers are

a class of hybrid porous materials composed of metal units joined by organic/inorganic linkers, in which the diversity of the organic/inorganic linkers and exquisite control over pore aperture size promise great potential for gas separation and purification.<sup>[16–18]</sup> However, compared to the separation of CO<sub>2</sub>

Dr. X. L. Cui, Dr. Q. W. Yang, L. F. Yang, Dr. Z. G. Zhang, Dr. Z. B. Bao, Prof. Q. L. Ren, Prof. H. B. Xing  
Key Laboratory of Biomass Chemical Engineering of Ministry of Education  
College of Chemical and Biological Engineering  
Zhejiang University  
Hangzhou 310027, China  
E-mail: yangqw@zju.edu.cn; xinghb@zju.edu.cn  
Prof. R. Krishna  
Van't Hoff Institute for Molecular Sciences  
University of Amsterdam  
Science Park 904, Amsterdam 1098 XH, The Netherlands

Dr. H. Wu, Prof. W. Zhou  
Center for Neutron Research  
National Institute of Standards and Technology  
Gaithersburg, MD 20899-6102, USA  
Prof. B. L. Chen  
Department of Chemistry  
University of Texas at San Antonio  
One UTSA Circle  
San Antonio, TX 78249-0698, USA  
E-mail: banglin.chen@utsa.edu

 The ORCID identification number(s) for the author(s) of this article can be found under <https://doi.org/10.1002/adma.201606929>.

DOI: 10.1002/adma.201606929

and hydrocarbons,<sup>[19–29]</sup> the selective adsorption of SO<sub>2</sub> has rarely been studied on MOFs, especially the adsorption at low partial pressures that is actually needed by the gas desulfurization.<sup>[30–36]</sup> Generally, the desulfurization of flue gas is a step before CO<sub>2</sub> scrubbing process, however, few work paid attention to the selective removal of SO<sub>2</sub> from CO<sub>2</sub>. In fact, considering the acidic nature of both SO<sub>2</sub> and CO<sub>2</sub> molecules and the much lower SO<sub>2</sub> concentration in flue gas than CO<sub>2</sub> (CO<sub>2</sub>: 10–12%, v/v; SO<sub>2</sub>: about 2000 ppm), it is very challenging to remove SO<sub>2</sub> from CO<sub>2</sub> with high selectivity.<sup>[37,38]</sup> These abovementioned problems prompted us to develop advanced porous materials with delicate structure and chemistry for the adsorption of SO<sub>2</sub>, and elucidate the way in which contributions such as pore size and pore surface electrostatic environment enhance the selective recognition of SO<sub>2</sub> with high uptake capacity.

In this work, we for the first time reported the selective recognition and dense packing of the so-called “SO<sub>2</sub> cluster” using hybrid porous materials through precisely tuning the pore size and pore chemistry. Featuring copper coordination networks with inorganic hexafluorosilicate (SiF<sub>6</sub><sup>2-</sup>, SIFSIX) anions and organic linkers, SIFSIX-1-Cu (1 = 4,4'-bipyridine)<sup>[24]</sup> and SIFSIX-2-Cu-i (2 = 4,4'-dipyridylacetylene, i = interpenetrated)<sup>[19]</sup> contain pore spaces that enable high SO<sub>2</sub> uptake with specific recognition and afford new benchmarks for the highly efficient removal of SO<sub>2</sub> from other gases. Not only extraordinary ambient uptake of SO<sub>2</sub> was achieved with SIFSIX-1-Cu as adsorbent, but also unprecedented low-pressure SO<sub>2</sub> capacity was attained with SIFSIX-2-Cu-i. Moreover, record SO<sub>2</sub>/CO<sub>2</sub> selectivity and excellent SO<sub>2</sub>/N<sub>2</sub> selectivity were also exhibited by the SIFSIX materials. We attribute this exceptional performance to the synergistic guest–host interactions (S<sup>δ+</sup>...F<sup>δ-</sup> and O<sup>δ-</sup>...H<sup>δ+</sup> interactions) that firmly grasp every atom of SO<sub>2</sub> in the pores of SIFSIX materials along with the considerable guest–guest interactions among SO<sub>2</sub> molecules and the optimal

pore size, which together enable the preferential binding and cluster formation of SO<sub>2</sub> in the pores densely.

These SIFSIX materials exhibit a pillared square-grid 3D structure with inorganic SiF<sub>6</sub><sup>2-</sup> ions as a linear bridge between transition-metal moieties. Previously, we have succeeded in the specific recognition of acetylene from ethylene using SIFSIX materials.<sup>[39]</sup> In this work, we systematically studied the adsorption of SO<sub>2</sub> on SIFSIX-1-Cu, SIFSIX-2-Cu (2, 4,4'-dipyridylacetylene), SIFSIX-2-Cu-i, SIFSIX-3-Zn (3,pyrazine), and SIFSIX-3-Ni at atmospheric and low pressures. At first, the uptake capacity of SO<sub>2</sub> as single-component gas on activated SIFSIX-1-Cu, SIFSIX-2-Cu, SIFSIX-2-Cu-i, SIFSIX-3-Zn, and SIFSIX-3-Ni were determined at 298 K and 1.01 bar (Table 1). Remarkably, SIFSIX-1-Cu exhibited superb adsorption capacity (11.01 mmol g<sup>-1</sup>) among SIFSIX materials, while SIFSIX-2-Cu-i and SIFSIX-2-Cu uptake 6.90 and 6.50 mmol g<sup>-1</sup>, respectively (Table 1). To the best of our knowledge, this extraordinarily high value of 11.01 mmol g<sup>-1</sup> measured at room temperature and ambient pressure is the highest of all the materials reported under the same condition so far, including top-performing ones such as M(bdc)(ted)<sub>0.5</sub> (9.97 mmol g<sup>-1</sup>),<sup>[36]</sup> NOTT-300 (Al) (7.1 mmol g<sup>-1</sup>),<sup>[34]</sup> MFM-300(In) (8.28 mmol g<sup>-1</sup>),<sup>[35]</sup> and MFM-202a (10.2 mmol g<sup>-1</sup>).<sup>[33]</sup>

The adsorption isotherms of SO<sub>2</sub> at 298 and 273 K on SIFSIX materials were measured to systematically demonstrate the SO<sub>2</sub> capture ability of these materials at low pressures (Figure 1 and Table 1), as needed by the actual desulfurization process due to the low SO<sub>2</sub> concentration in feed gas. Notably, the measurements were performed using SO<sub>2</sub>/N<sub>2</sub> mixed gas with varying SO<sub>2</sub> molar fractions under flow mode.

As can be noted from Figure 1A, the adsorption isotherms of SO<sub>2</sub> on SIFSIX-1-Cu, SIFSIX-2-Cu-i, SIFSIX-3-Ni, and SIFSIX-3-Zn show a steep increase in the low-pressure range and then reach saturation. At an extremely low SO<sub>2</sub> partial pressure of

**Table 1.** The adsorption capacities of SO<sub>2</sub> in various porous materials at different partial pressure of SO<sub>2</sub>. Summary of the adsorption collected at 298 K. Note: The SO<sub>2</sub> adsorption capacities at 0.002, 0.01, and 0.1 bar were determined using SO<sub>2</sub>/N<sub>2</sub> mixed gas with varying SO<sub>2</sub> molar fractions under flow mode, while the SO<sub>2</sub> adsorption capacities at 1.0 bar were determined using SO<sub>2</sub> pure gas.

| Materials                                   | SO <sub>2</sub> uptake [mmol g <sup>-1</sup> ] |                        |                       |                   | Selectivity for SO <sub>2</sub> /CO <sub>2</sub> at 10/90 mixture | Selectivity for SO <sub>2</sub> /N <sub>2</sub> at 10/90 mixture | Selectivity for SO <sub>2</sub> /CH <sub>4</sub> at 10/90 mixture | Q <sub>st</sub> [SO <sub>2</sub> kJ mol <sup>-1</sup> ] |
|---|--|------------------------|-----------------------|-------------------|---|--|---|---|
|   | 0.002 bar <sup>a)</sup>                        | 0.01 bar <sup>a)</sup> | 0.1 bar <sup>a)</sup> | 1.0 bar           |   |  |   |   |
| SIFSIX-1-Cu                                 | 1.80   | 3.43                   | 8.74                  | 11.01             | 70.7  | 3145.7   | 1241.4  | 36.1  |
| SIFSIX-2-Cu-i                               | 2.31   | 4.16                   | 6.01                  | 6.90              | 87.1  | 3103.2   | 1017.1  | 38.1  |
| SIFSIX-3-Zn                                 | 0.98   | 1.68                   | 1.89                  | 2.10              | –   | 506.7  | 276.0   | 45.2  |
| SIFSIX-3-Ni                                 | 1.39   | 2.43                   | 2.55                  | 2.74              | –   | 701.8  | 371.6   | 43.2  |
| SIFSIX-2-Cu                                 | –  | –                      | –                     | 6.50              | –   | –  | –   | –   |
| Ni(bdc)(ted) <sub>0.5</sub> <sup>[36]</sup> | –  | –                      | 3.50                  | 9.97              | –   | –  | –   | –   |
| Zn-MOF-74 <sup>[30]</sup>                   | –  | 3.03 <sup>b)</sup>     | –                     | –                 | –   | –  | –   | –   |
| MFM-300(In) <sup>[35]</sup>                 | –  | –                      | –                     | 8.28              | 50 <sup>d)</sup>  | 2700 <sup>d)</sup>   | –   | 34.5/39.6 <sup>e)</sup>                                 |
| MFM-202a <sup>[33]</sup>                    | –  | –                      | 3.0                   | 10.2              | –   | –  | –   | 35  |
| NOTT-300 (Al) <sup>[34]</sup>               | –  | –                      | –                     | 7.1 <sup>f)</sup> | –   | –  | –   | –   |
| P(TMGA-co-MBA) <sup>[40]</sup>              | –  | –                      | –                     | 4.06              | –   | –  | –   | –   |
| Activated Carbon <sup>[41]</sup>            | –  | –                      | –                     | 3.3 <sup>c)</sup> | –   | –  | –   | –   |

<sup>a)</sup>Partial pressure of SO<sub>2</sub>; <sup>b)</sup>Dynamic adsorption capacity; <sup>c)</sup>At the temperature of 323 K and pressure of 0.46 bar; <sup>d)</sup>These data were read from the figures of ref. [35]; <sup>e)</sup>Highest Q<sub>st</sub> values at different surface coverage; <sup>f)</sup>At the temperature of 298 K.

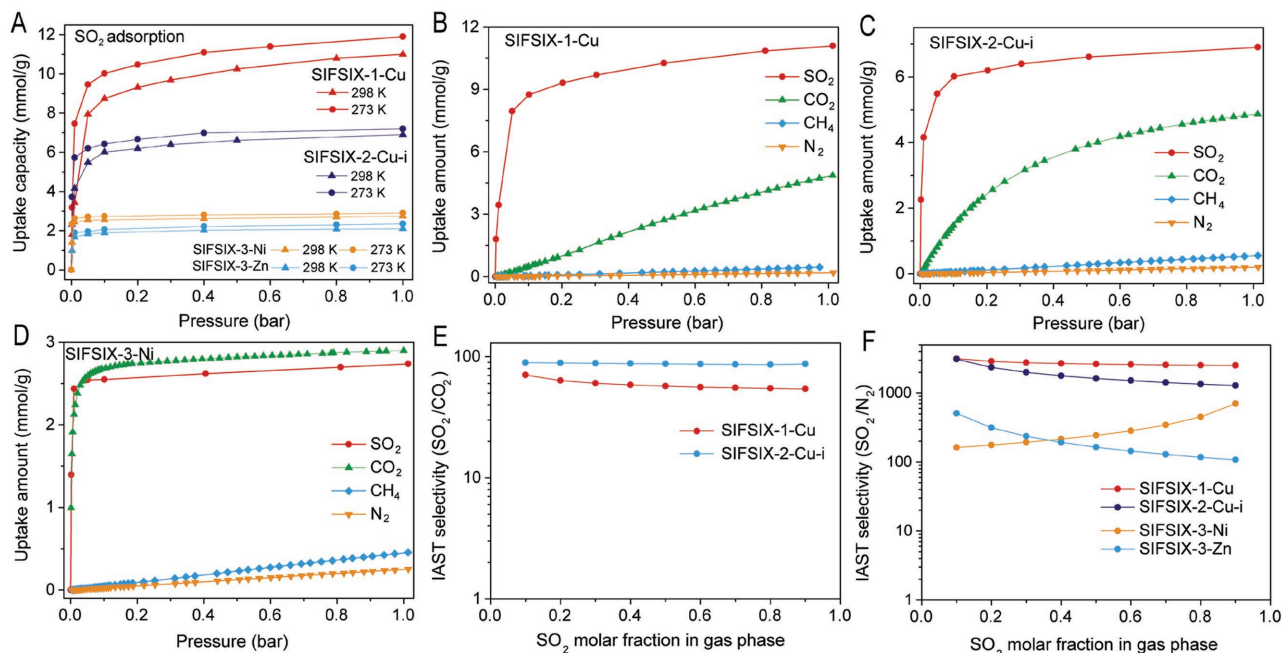


**Figure 1.** A) SO<sub>2</sub> adsorption isotherms of SIFSIX-1-Cu, SIFSIX-2-Cu-i, SIFSIX-3-Zn, and SIFSIX-3-Ni at 273 and 298 K. Adsorption isotherms for SO<sub>2</sub>, CO<sub>2</sub>, CH<sub>4</sub> and N<sub>2</sub> on B) SIFSIX-1-Cu, C) SIFSIX-2-Cu-i, and D) SIFSIX-3-Ni at 298 K. Note: SO<sub>2</sub> isotherms were measured using SO<sub>2</sub>/N<sub>2</sub> mixed gas with varying SO<sub>2</sub> molar fractions under flow mode. CO<sub>2</sub>, CH<sub>4</sub>, and N<sub>2</sub> isotherms were measured using single-component gas. IAST selectivities of SIFSIX materials with E) SO<sub>2</sub>/CO<sub>2</sub> mixtures and F) SO<sub>2</sub>/N<sub>2</sub> mixtures with varying SO<sub>2</sub> molar fractions in gas phase at 100 kPa.

0.002 bar (2000 ppm) and 298 K, SIFSIX-2-Cu-i rapidly uptake as high as 2.31 mmol g<sup>-1</sup> SO<sub>2</sub> (Figure 1C and Table 1), exceeding the capacity of SIFSIX-1-Cu (1.80 mmol g<sup>-1</sup>), SIFSIX-3-Zn (0.98 mmol g<sup>-1</sup>), and SIFSIX-3-Ni (1.39 mmol g<sup>-1</sup>) (Figure 1B,D and Table 1). This excellent capacity of SO<sub>2</sub> at such a low pressure indicates that SIFSIX-2-Cu-i has great potential in FGD applications. At 298 K, when the partial pressure of SO<sub>2</sub> increased to 0.01 bar, the SO<sub>2</sub> uptake of SIFSIX-2-Cu-i rose to 4.16 mmol g<sup>-1</sup> SO<sub>2</sub>, not only still higher than the other three SIFSIX materials but also exceeding the benchmark uptake of Zn-MOF-74 (3.03 mmol g<sup>-1</sup>). As the pressure of SO<sub>2</sub> further increased to 0.1 bar, the uptake amount of SO<sub>2</sub> at 298 K on SIFSIX-1-Cu increased more rapidly and became more than that on SIFSIX-2-Cu-i, approaching a value of 8.74 mmol g<sup>-1</sup> while SIFSIX-2-Cu-i exhibits 6.01 mmol g<sup>-1</sup>, both higher than that ever reported under the same conditions (3.5 mmol g<sup>-1</sup> by Ni(bdc)(ted)<sub>0.5</sub>). When the temperature decreased to 273 K, a steep increase in the low-pressure range of isotherms to a high SO<sub>2</sub> capacity was still observed on all these five SIFSIX materials. As shown in Figure 1A, at 273 K and the low SO<sub>2</sub> partial pressure of 0.002 bar, SIFSIX-2-Cu-i exhibited remarkable higher uptake of SO<sub>2</sub> (3.72 mmol g<sup>-1</sup>), exceeding SIFSIX-1-Cu (3.18 mmol g<sup>-1</sup>) and SIFSIX-3-Ni (2.34 mmol g<sup>-1</sup>). With the increase of SO<sub>2</sub> partial pressure, SIFSIX-1-Cu exhibited higher uptake than SIFSIX-2-Cu-i, SIFSIX-3-Ni, and SIFSIX-3-Zn within the whole range of 0.01–1.01 bar. Overall, the results in Table 1 and Figure 1A demonstrate that exceptional SO<sub>2</sub> capacity can be afforded by SIFSIX materials from atmospheric to very low pressures, even more superior at low pressures.

To evaluate the selectivity of SO<sub>2</sub> to other typical gases in gas desulfurization processes, adsorption isotherms of CO<sub>2</sub>, CH<sub>4</sub>,

and N<sub>2</sub> on SIFSIX materials were collected at 298 K using pure gas. Although both CO<sub>2</sub> and SO<sub>2</sub> are acidic gases, the CO<sub>2</sub> isotherms on SIFSIX-1-Cu show dramatically different adsorption behaviors than SO<sub>2</sub> adsorption isotherms (Figure 1B,C). These dramatic differences between SO<sub>2</sub> and CO<sub>2</sub> adsorption behavior and capacity, especially at low pressures, offer a great potential of selective recognition of SO<sub>2</sub> toward CO<sub>2</sub> on SIFSIX-1-Cu and SIFSIX-2-Cu-i. In addition, SIFSIX-1-Cu and SIFSIX-2-Cu-i only adsorbed 0.45 and 0.55 mmol g<sup>-1</sup> CH<sub>4</sub> at 298 K and 1.0 bar (Figure 1A,B), respectively, which are negligible compared to SO<sub>2</sub> uptake capacity. Furthermore, the uptake amount of N<sub>2</sub> was much lower than CH<sub>4</sub> (Figure 1B–D). As for the case of SIFSIX-3-Ni (Figure 1D) and SIFSIX-3-Zn (Figure S4, supporting information), the CO<sub>2</sub> capacity was higher than the SO<sub>2</sub> capacity, and CH<sub>4</sub> and N<sub>2</sub> were still rarely adsorbed.

In order to further address the separation capability of SIFSIX materials in different gas desulfurization processes, SO<sub>2</sub>/CO<sub>2</sub> and SO<sub>2</sub>/N<sub>2</sub> separation selectivity were determined using ideal adsorbed solution theory (IAST) calculations as a function of varying SO<sub>2</sub> composition (from 0.1 to 0.9).<sup>[42,43]</sup> Notably, in these IAST calculations, the SO<sub>2</sub> isotherms on SIFSIX materials were measured using SO<sub>2</sub>/N<sub>2</sub> mixed gas, which might slightly underestimate the selectivity. As shown in Figure 1E, SIFSIX-1-Cu shows excellent SO<sub>2</sub>/CO<sub>2</sub> separation selectivity (54–70) over a wide range of SO<sub>2</sub> molar fraction in gas phase (0.1–0.9), especially in the low concentration range. Even better, SIFSIX-2-Cu-i exhibits record SO<sub>2</sub>/CO<sub>2</sub> selectivity (86–89) within 0.1–0.9 molar fraction of SO<sub>2</sub>. Considering the fact of low SO<sub>2</sub> concentration in typical flue gas (SO<sub>2</sub>/CO<sub>2</sub>/N<sub>2</sub>), this large SO<sub>2</sub>/CO<sub>2</sub> selectivity endows SIFSIX-1-Cu and SIFSIX-2-Cu-i with potential in FGD process. This is crucial to realize

a thorough removal of trace SO<sub>2</sub> from flue gas before the CO<sub>2</sub> scrubbing process to ensure the activity of CO<sub>2</sub> adsorbent. To the best of our knowledge, the SO<sub>2</sub>/CO<sub>2</sub> IAST selectivity on SIFSIX-2-Cu-i (86–89) and SIFSIX-1-Cu (54–70) sets new benchmarks for SO<sub>2</sub>/CO<sub>2</sub> separation. The separation selectivities of SO<sub>2</sub>/N<sub>2</sub> and SO<sub>2</sub>/CH<sub>4</sub> on the SIFSIX materials were as well estimated by IAST. Figure 1 F shows the high SO<sub>2</sub>/N<sub>2</sub> selectivities on SIFSIX-1-Cu (2510–3145) and SIFSIX-2-Cu-i (1285–3103) over a wide range of SO<sub>2</sub> molar fraction in gas phase (0.1–0.9). Moreover, high SO<sub>2</sub>/CH<sub>4</sub> selectivities (Figure S5, Supporting Information) over the same range of SO<sub>2</sub> molar fraction were also achieved on SIFSIX-1-Cu (992–1241), SIFSIX-2-Cu-i (422–1017), and SIFSIX-3-Ni (86–371). Therefore, SIFSIX-1-Cu and SIFSIX-2-Cu-i fulfill the requirements by FGD technology, natural-gas purification and other SO<sub>2</sub>-separation processes for both SO<sub>2</sub> capacity and selectivity.

To unravel the nature of the interactions between SO<sub>2</sub> molecule and SIFSIX materials, we performed modeling studies using first-principles DFT-D (dispersion-corrected density functional theory) calculations. When trapped within the pore of SIFSIX-1-Cu, SO<sub>2</sub> gets adsorbed primarily through the S<sup>δ+</sup>...F<sup>δ-</sup> electrostatic interaction (Figure 2) with SiF<sub>6</sub><sup>-</sup> anion and the multiple O<sup>δ-</sup>...H<sup>δ+</sup> dipole–dipole interactions with the 4,4′-bipyridine linker (Figure 2B). The DFT-D calculated S...F distance is ≈2.6 Å (Figure 2A), much smaller than the sum of the van der Waals radii of S and F (3.3 Å), indicating the considerable strength of this interaction that arises from the negative nature of SiF<sub>6</sub><sup>2-</sup> ion and positive charge of S atom. Simultaneously, the two oxygen atoms of SO<sub>2</sub> molecule are bonded by the 4,4′-bipyridine linker through multiple dipole–dipole interactions, especially the O<sup>δ-</sup>...H<sup>δ+</sup> interactions between oxygen atoms and aromatic hydrogens with a distance of 2.39–3.30 Å (Figure 2B). These multiple synergistic interactions enable the specific recognition of SO<sub>2</sub> molecules through grasping every atoms of the adsorbed SO<sub>2</sub>, with a calculated strong adsorption energy (ΔE) of 50.3 kJ mol<sup>-1</sup>. Thanks to the four equivalent F sites and four equivalent aromatic linkers, four SO<sub>2</sub> molecules were trapped firmly by the host–guest S<sup>δ+</sup>...F<sup>δ-</sup> and O<sup>δ-</sup>...H<sup>δ+</sup> interactions per unit cell. After that, it is noticed that there are still occupiable pore space in the unit

cell of SIFSIX-1-Cu (between the F sites, along crystallography *c* direction) to accommodate more SO<sub>2</sub> guests. DFT-D calculations showed that two more SO<sub>2</sub> molecules could be trapped in this space as the secondary adsorption, through the dipole–dipole interactions with the channel pore surface and the intermolecular interaction (mainly dipole–dipole interaction) with the SO<sub>2</sub> adsorbed at the primary sites. The ΔE of SO<sub>2</sub> on this site was 38.7 kJ mol<sup>-1</sup>, with a calculated nearest S<sub>site2</sub>...O<sub>site1</sub> distance of 3.6 Å. As a result, six SO<sub>2</sub> were trapped within per unit cell of SIFSIX-1-Cu, four of which were primarily adsorbed via host–guest interactions and the other two were secondarily accommodated mainly via guest–guest interaction with the primary SO<sub>2</sub>.

Previous studies have shown that the intermolecular distance in SO<sub>2</sub> liquid tested from X-ray diffraction and neutron studies were centered at 3.5, 4.5, and 5.6 Å with different types of orientations.<sup>[44,45]</sup> As clearly shown in Figure 2A, the intermolecular distance of adsorbed SO<sub>2</sub>(I) and SO<sub>2</sub>(II) is 3.32, 3.56, and 4.07 Å, respectively, within the distance range of the liquid SO<sub>2</sub>. These abovementioned data visualize the dense packing of “SO<sub>2</sub> clusters” within the confined electrostatic nanospace of SIFSIX-1-Cu, in consequence of the synergistic host–guest and guest–guest interactions. It is worth noting that this dense packing of “SO<sub>2</sub> clusters” at ambient temperature and low pressure has rarely been reported in common porous adsorbents.

The dense packing of SO<sub>2</sub> clusters within SIFSIX materials is not only the result of the unique pore chemistry but also the optimal pore size. When the organic linker in SIFSIX-1-Cu was replaced by a longer analog, 4,4′-dipyridylacetylene, the resulted SIFSIX-2-Cu showed a weaker interaction with SO<sub>2</sub> (44.2 kJ mol<sup>-1</sup>) than SIFSIX-1-Cu. The S...F electrostatic interaction was basically of the same nature and strength in the two isoreticular MOFs, implied by the very similar S...F distances, but the dipole–dipole interaction between SO<sub>2</sub> and the 4,4′-dipyridylacetylene linker was slightly weaker than the 4,4′-bipyridine case because of the larger channel pore size of this SIFSIX material. The experimental SO<sub>2</sub> capacity of SIFSIX-2-Cu at room temperature and 1 bar was 6.5 mmol g<sup>-1</sup>, equivalent to ≈3.7 SO<sub>2</sub> per unit cell. This is lower than the capacity of SIFSIX-1-Cu that was 11.0 mmol g<sup>-1</sup> and equivalent to

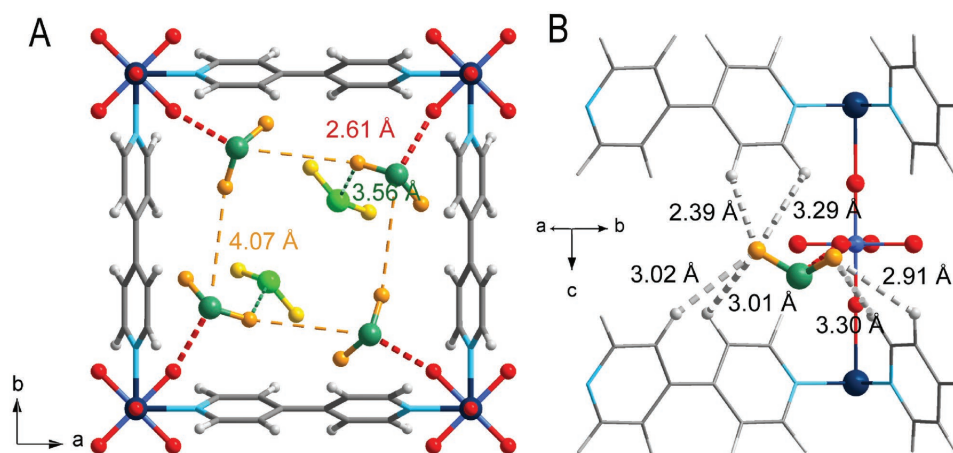


**Figure 2.** A,B) DFT-D calculated SO<sub>2</sub> adsorption binding sites in SIFSIX-1-Cu viewing in two different directions. Color code: F, red; Si, light blue; C, gray; H, light gray; N, sky blue; Cu, dark teal; O, orange; S, sea green (Note: the secondary adsorbed SO<sub>2</sub> molecules were highlighted with bright color).

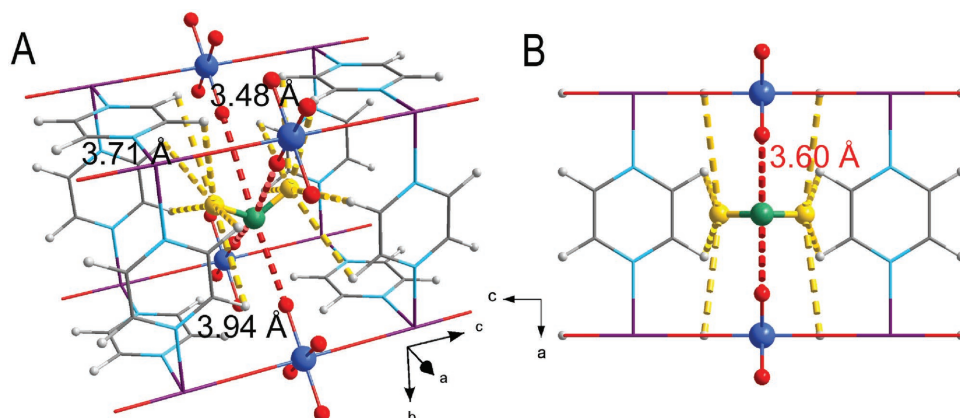


**Figure 3.** A,B) DFT-D calculated  $\text{SO}_2$  adsorption binding sites in SIFSIX-3-Zn viewing in two different directions. Color code: F, red; Si, light blue; C, gray; H, light gray; N, sky blue; Zn, violet; O, orange; S, sea green.

$\approx 5.7$   $\text{SO}_2$  per unit cell. A too small pore size also goes against the uptake of  $\text{SO}_2$ . In SIFSIX-3-Zn, the channel pore size is small due to the much shorter linker pyrazine. DFT-D calculations show that  $\text{SO}_2$  molecules get preferentially adsorbed at the center of the 1D channel of SIFSIX-3-Zn along the crystallography  $c$ -axis. Although the calculated  $\Delta E$  of  $\text{SO}_2$  with SIFSIX-3-Zn was  $54.1 \text{ kJ mol}^{-1}$ , slightly higher than that in SIFSIX-1-Cu, the much smaller pore volume captured less  $\text{SO}_2$  than SIFSIX-1-Cu. The much longer  $\text{S} \cdots \text{F}$  distance ( $3.60 \text{ \AA}$ ) demonstrates a weaker  $\text{S}^{\delta+} \cdots \text{F}^{\delta-}$  interaction between  $\text{SO}_2$  and SIFSIX-3-Zn (Figure 3) than the SIFSIX-1-Cu case, and the grasp of one  $\text{SO}_2$  in SIFSIX-3-Zn consumes four times as much F sites as in SIFSIX-1-Cu.

The significance of a well-designed pore chemistry and pore size on the dense packing of  $\text{SO}_2$  clusters was further highlighted by the modeling on SIFSIX-2-Cu-i. Although the organic linker in SIFSIX-2-Cu-i is the same as that in SIFSIX-2-Cu, the framework interpenetration in SIFSIX-2-Cu-i enables the size of its unit cell approximately half of that of SIFSIX-2-Cu with a more compact  $\text{SiF}_6^{2-}$  distribution (Figure 4). DFT-D calculation showed that the  $\text{S} \cdots \text{F}$  distance in this MOF is  $\approx 2.44 \text{ \AA}$ , lower than those in other modeled SIFSIX materials, indicating a strong  $\text{S}^{\delta+} \cdots \text{F}^{\delta-}$  electrostatic interaction between  $\text{SO}_2$  and  $\text{SiF}_6^{2-}$ . On the other hand, the two O atoms of  $\text{SO}_2$  interact with the H atoms of 4,4'-dipyridylacetylene through multiple

$\text{O}^{\delta-} \cdots \text{H}^{\delta+}$  interactions, with  $\text{O} \cdots \text{H}$  distances of  $2.79\text{--}3.34 \text{ \AA}$  (Figure 4A). In consequence, every atom of the adsorbed  $\text{SO}_2$  was grasped by the pore surface of SIFSIX-2-Cu-i through these multiple synergistic host-guest interactions, with a  $\Delta E$  of  $\approx 50.2 \text{ kJ mol}^{-1}$ . This is comparable to that in SIFSIX-1-Cu ( $\approx 50.3 \text{ kJ mol}^{-1}$ ). The two  $\text{SiF}_6^{2-}$  anions on the diagonal of each unit cell in SIFSIX-2-Cu-i enables the adsorption of two  $\text{SO}_2$  by the host-guest  $\text{S}^{\delta+} \cdots \text{F}^{\delta-}$  and  $\text{O}^{\delta-} \cdots \text{H}^{\delta+}$  interactions. Interestingly, because those two  $\text{SO}_2$  molecules are located very close to each other, with the nearest  $\text{S} \cdots \text{O}$  distance of only  $\approx 3.2 \text{ \AA}$ , which enhance the guest-guest interactions (Figure 4A,B). The cooperation of the host-guest and guest-guest interactions affords the formation of  $\text{SO}_2$  clusters within the confined electrostatic nanospace of SIFSIX-2-Cu-i. The nearest  $\text{S} \cdots \text{O}$  distance of  $\approx 3.2 \text{ \AA}$  between two neighboring adsorbed  $\text{SO}_2$  is comparable to the intermolecular distance ( $3.5\text{--}5.6 \text{ \AA}$ ) in liquid crystal  $\text{SO}_2$  phase and even slightly smaller than that in SIFSIX-1-Cu, implying a dense packing of  $\text{SO}_2$  clusters within the pores of SIFSIX-2-Cu-i that enables the excellent uptake of  $\text{SO}_2$  at low partial pressures. As presented in Table 1, the experimental  $\text{SO}_2$  adsorption capacity of SIFSIX-2-Cu-i at room temperature and  $0.01 \text{ bar}$  was as large as  $4.16 \text{ mmol g}^{-1}$ , much higher than those in SIFSIX-1-Cu ( $3.43 \text{ mmol g}^{-1}$ ), SIFSIX-3-Zn and SIFSIX-3-Ni. Even if at  $0.002 \text{ bar}$  ( $2000 \text{ ppm}$ ) the  $\text{SO}_2$  capacity was as high as  $2.26 \text{ mmol g}^{-1}$ . Overall, DFT-D calculations on the different

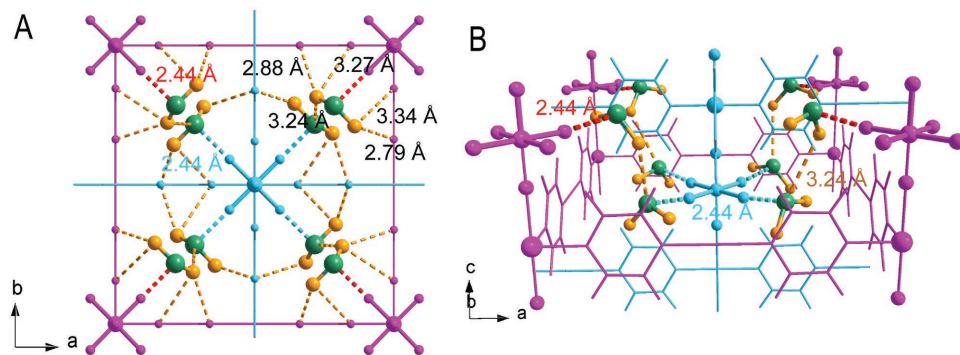


**Figure 4.** A,B) DFT-D calculated  $\text{SO}_2$  adsorption sites in SIFSIX-2-Cu-i viewing in two different directions, and C) crystal structure obtained from Rietveld refinement of PXRD data on  $\text{SO}_2$ -loaded SIFSIX-2-Cu-i. (Note: the different nets are highlighted in magenta and cyan for clarity).

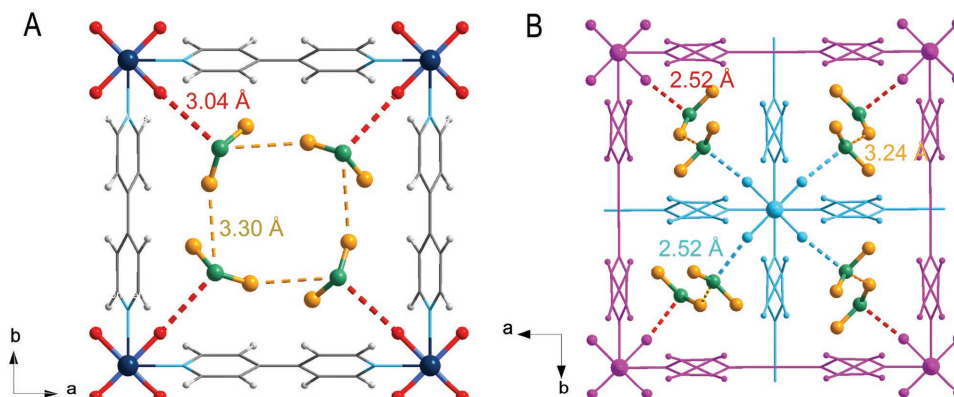


**Figure 5.** A,B) Crystal structure obtained from Rietveld refinement of PXRD data on  $\text{SO}_2$ -loaded SIFSIX-1-Cu (A) and SIFSIX-2-Cu-i (B).

SIFSIX materials manifest that the excellent  $\text{SO}_2$  capture performance of SIFSIX-1-Cu and SIFSIX-2-Cu-i can be attributed to the synergetic host–guest binding (electrostatic and dipole–dipole interactions) and cooperative guest–guest interactions within the confined electrostatic nanospace of moderate size to form  $\text{SO}_2$  clusters.

To provide experimental proof for the DFT-D analysis of  $\text{SO}_2$ -SIFSIX interactions, we have performed Rietveld refinement of the powder X-ray diffraction patterns of  $\text{SO}_2$ -loaded samples to locate the adsorbed positions of  $\text{SO}_2$  molecules in the crystal structure of SIFSIX materials, and the experimental results are well consistent with the DFT-D calculation results. The Rietveld refined data reveals that in the interpenetrated structure of SIFSIX-2-Cu-i, each  $\text{SO}_2$  molecule indeed interacts with SIFSIX-2-Cu-i through  $\text{S}^{\delta+}\cdots\text{F}^{\delta-}$  bonding (2.52 Å) and multiple  $\text{O}^{\delta-}\cdots\text{H}^{\delta+}$  interactions (Figure 5B). The nearest  $\text{S}\cdots\text{O}$  distance between adjacent  $\text{SO}_2$  molecules are 3.2 Å. In SIFSIX-1-Cu,  $\text{SO}_2$  also gets adsorbed primarily through the  $\text{S}^{\delta+}\cdots\text{F}^{\delta-}$  electrostatic interaction with  $\text{SiF}_6^-$  anion (Figure 5A). The  $\text{S}^{\delta+}\cdots\text{F}^{\delta-}$  distance is 3.04 Å, longer than the modeling results (2.61 Å). Cooperative interactions between adjacent  $\text{SO}_2$  molecules are also observed in the crystal structure of SIFSIX-1-Cu· $\text{SO}_2$  with a  $\text{S}\cdots\text{O}$  distance of 3.3 Å.

We also have performed the detailed DFT-D calculations for  $\text{CO}_2/\text{N}_2$  molecules to illustrate the difference on interactions between  $\text{SO}_2$  and  $\text{N}_2/\text{CO}_2$  molecules. Results show that the calculated  $\text{C}\cdots\text{F}$  distances between  $\text{CO}_2$  and  $\text{SiF}_6^{2-}$  (2.52 and 2.80 Å) in SIFSIX-2-Cu-i (Figure S10, Supporting Information) are longer than those between  $\text{SO}_2$  and  $\text{SiF}_6^{2-}$  binding sites (2.44 Å), indicating that SIFSIX-2-Cu-i interacted more strongly with  $\text{SO}_2$  than  $\text{CO}_2$ . In SIFSIX-1-Cu, the calculated  $\text{C}\cdots\text{F}$  distance for  $\text{CO}_2$  (2.60 Å) is comparable to the  $\text{S}\cdots\text{F}$  distance for  $\text{SO}_2$  (2.61 Å); however, the calculated  $\text{O}\cdots\text{H}$  distances between  $\text{CO}_2$  molecule and 4,4'-bipyridine (2.64–3.58 Å) are longer than that of  $\text{SO}_2$  system (2.39–3.30 Å) (Figure S11, Supporting Information). Additionally, the static adsorption energy ( $\Delta E$ ) results show that there are much stronger interactions with  $\text{SO}_2$  than  $\text{CO}_2$  ( $\Delta E$  in SIFSIX-2-Cu-i, 50.2 versus 35.7  $\text{kJ mol}^{-1}$ ;  $\Delta E$  in SIFSIX-1-Cu, 50.3 vs 31.1  $\text{kJ mol}^{-1}$ ;  $\Delta E$  in SIFSIX-3-Zn, 54.1 versus 45.7  $\text{kJ mol}^{-1}$ ).

To confirm the actual  $\text{SO}_2/\text{N}_2$  and  $\text{SO}_2/\text{CO}_2$  separation performance on the SIFSIX materials, we conducted experimental breakthrough tests at 298 K and 1.01 bar on SIFSIX-2-Cu-i, SIFSIX-1-Cu, and SIFSIX-3-Ni (Figure 6).  $\text{SO}_2/\text{N}_2$  mixture

containing 2000 ppm  $\text{SO}_2$  was used to mimic the flue gas with low concentration of  $\text{SO}_2$ . The reason for using SIFSIX-3-Ni rather than SIFSIX-3-Zn is the relatively higher stability of SIFSIX-3-Ni (Figure S15, Supporting Information). As shown in Figure 6A, highly efficient elimination of  $\text{SO}_2$  was achieved with clean  $\text{N}_2$  eluted from the bed by all the three SIFSIX materials. The breakthrough time of  $\text{SO}_2$  on SIFSIX-2-Cu-i (1800  $\text{min g}^{-1}$ ) exceeded that on SIFSIX-1-Cu and SIFSIX-3-Ni, consistent with the higher  $\text{SO}_2$  adsorption capacities of SIFSIX-2-Cu-i (2.31  $\text{mmol g}^{-1}$ ) than SIFSIX-1-Cu (1.80  $\text{mmol g}^{-1}$ ) and SIFSIX-3-Ni (1.39  $\text{mmol g}^{-1}$ ) in static adsorption experiment at 298 K and 0.002 bar (Figure 1A). Additionally, the actual  $\text{SO}_2/\text{CO}_2$  separation performance on these SIFSIX materials was also confirmed by the breakthrough experiments, in which the  $\text{SO}_2/\text{CO}_2$  mixture containing 2000 ppm  $\text{SO}_2$  was used. As shown in Figure 6B, outstanding efficient separation of  $\text{SO}_2/\text{CO}_2$  was achieved with clean  $\text{CO}_2$  eluted from the bed by SIFSIX-1-Cu and SIFSIX-2-Cu-i, agreeing well with the results of adsorption isotherm and IAST calculations. The superb  $\text{SO}_2/\text{N}_2$  and  $\text{SO}_2/\text{CO}_2$  selectivity at very low  $\text{SO}_2$  concentrations makes SIFSIX materials very promising for the gas desulfurization applications.

Given that  $\text{SO}_2$  is highly corrosive and few porous MOF materials are stable to the presence of  $\text{SO}_2$ , concerns about material regeneration are raised. Therefore, we conducted cycling breakthrough tests to evaluate the reusability of SIFSIX-2-Cu-i and SIFSIX-1-Cu for  $\text{SO}_2$  capture. As the desorption curves shown in the Figure S16 (Supporting Information), SIFSIX materials adsorbed with  $\text{SO}_2$  could be fully regenerated by He flow at 313 K. The breakthrough performance of SIFSIX-2-Cu-i and SIFSIX-1-Cu for 0.2/99.8 ( $\text{SO}_2/\text{CO}_2$ ) mixture did not declined during 6 and 4 cycles, respectively (Figure 6C,D). And XRD patterns indicated that both of the SIFSIX materials retain their stability after breakthrough experiments (Figure S6, Supporting Information). In addition, moisture (1000 ppm) has slightly effect on the adsorption capacity of  $\text{SO}_2$  on SIFSIX-2-Cu-i (Figure S17, Supporting Information) and SIFSIX-2-Cu-i is stable when exposed to humidity (75%) (Figure S18, Supporting Information).

In summary, this work reports the selective recognition and dense packing of the so-called  $\text{SO}_2$  clusters in hybrid porous materials with inorganic-anion-pillared metal–organic framework for the first time. The multiple binding sites of anionic and aromatic linkers initiate the specific recognition of  $\text{SO}_2$  by host–guest interactions that grasp the every atom of  $\text{SO}_2$

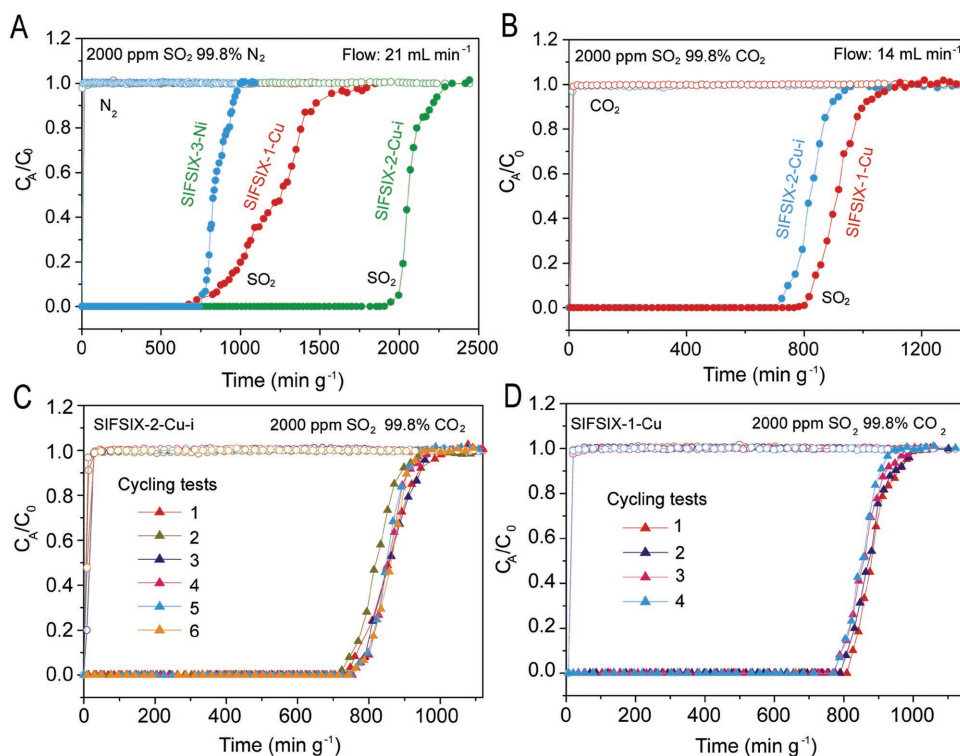


**Figure 6.** A,B) Experimental column breakthrough curves for SO<sub>2</sub>/N<sub>2</sub> (2000 ppm SO<sub>2</sub>) separations with SIFSIX-1-Cu, SIFSIX-2-Cu-i, and SIFSIX-3-Ni, and SO<sub>2</sub>/CO<sub>2</sub> (2000 ppm SO<sub>2</sub>) separations (A) and with SIFSIX-1-Cu and SIFSIX-2-Cu-i (B) at 298 K and 1.01 bar. C,D) Cycling column breakthrough tests for CO<sub>2</sub>/SO<sub>2</sub> (2000 ppm SO<sub>2</sub>) separations with SIFSIX-2-Cu-i (C) and SIFSIX-1-Cu (D) at 298 K and 1.01 bar (mixed gas flow: 14 mL min<sup>-1</sup>). In panel (A), open circles are for N<sub>2</sub>, and filled circles are for SO<sub>2</sub>. In panel (B), the open circles are for CO<sub>2</sub>, and the filled circles are for SO<sub>2</sub>. C<sub>A</sub>/C<sub>0</sub>, outlet concentration/feed concentration.

firmly, while the dipolar guest–guest interactions between SO<sub>2</sub> molecules enforce the adsorption through promoting the primary binding and enabling secondary adsorption to form SO<sub>2</sub> clusters. A moderate pore size is crucial to afford adequate strength of synergistic host–guest and guest–guest interactions for a dense packing of SO<sub>2</sub>. Thanks to the suitable pore chemistry and size, SIFSIX-1-Cu showed exceptionally high adsorption capacity of SO<sub>2</sub> (11.01 mmol g<sup>-1</sup> at 1.01 bar) and selectivity SIFSIX-2-Cu-i exhibited unprecedented SO<sub>2</sub> capacity at low pressures (4.16 mmol g<sup>-1</sup> at 0.01 bar and 2.31 mmol g<sup>-1</sup> at 0.002 bar) and record SO<sub>2</sub>/CO<sub>2</sub> selectivity (86–89), while SIFSIX-1-Cu showed exceptionally high adsorption capacity of SO<sub>2</sub> (11.01 mmol g<sup>-1</sup>) at 1.01 bar and also excellent SO<sub>2</sub>/CO<sub>2</sub> selectivity (54–70). Additionally, extraordinarily high SO<sub>2</sub>/N<sub>2</sub> selectivity was also achieved by SIFSIX-2-Cu-i (1285–3103) and SIFSIX-1-Cu (2510–3145). As further confirmed by the breakthrough experiments for mixed gases containing 2000 ppm SO<sub>2</sub>, this excellent performance sets a new benchmark in the highly efficient elimination of SO<sub>2</sub> from flue gas or natural gas even if with a low SO<sub>2</sub> concentration, and this work will be also instructive for the design of porous materials for other gas-purification processes.

## Experimental Section

**Materials:** SIFSIX materials including SIFSIX-1-Cu, SIFSIX-2-Cu, SIFSIX-2-Cu-i, SIFSIX-3-Zn, and SIFSIX-3-Ni were synthesized as

previously described in refs. [19] and [24] (see the Supporting Information for details).<sup>[19,24]</sup>

**SO<sub>2</sub> Adsorption:** SO<sub>2</sub> adsorption isotherms at 298 and 273 K were collected using the apparatus in Figure S1 (Supporting Information). Activated samples were packed in a glass container which was partly immersed in a water bath. The SO<sub>2</sub> adsorption isotherms were determined using SO<sub>2</sub>/N<sub>2</sub> mixed gas with varying SO<sub>2</sub> molar fractions under flow mode. Note: the adsorption of SO<sub>2</sub> at 1.01 bar was measured with pure SO<sub>2</sub> at flow mode. At the beginning of this experiment, the activated sample was loaded in the glass container which was full of pure N<sub>2</sub> atmosphere at 760 mmHg. Then, the SO<sub>2</sub>/N<sub>2</sub> mixed gas (e.g., 0.002/99.998) was introduced at a constant flow at 760 mmHg. Adsorption equilibrium was reached until the weight of glass container kept constant and did not change. The SO<sub>2</sub> uptake was calculated based on the weight change before and after dynamic adsorption (see the Supporting Information for more detailed adsorption procedures).

**Breakthrough Tests:** The breakthrough experiments were carried out in a dynamic gas breakthrough equipment (see Figure S2 in the Supporting Information).<sup>[39]</sup> All experiments were conducted using a stainless steel column (4.6 mm inner diameter × 50 mm). According to the different particle size and density of the sample powder, the weight packed in the column was: SIFSIX-1-Cu powder (0.21 g), SIFSIX-2-Cu-i (0.21 g), and SIFSIX-3-Ni (0.50 g), respectively. The column packed with sample was first purged with He flow (15 mL min<sup>-1</sup>) for 12 h at room temperature (25 °C). The mixed gas of SO<sub>2</sub>/N<sub>2</sub> = 0.2/99.8 (v/v) was then introduced at 21 mL min<sup>-1</sup>, and SO<sub>2</sub>/CO<sub>2</sub> = 0.2/99.8 (v/v) was introduced at 14 mL min<sup>-1</sup>. Outlet gas from the column was monitored using gas chromatography (GC-2010 plus) with a thermal conductivity detector (TCD) coupled with a FID. The gas mixture was separated by a capillary column (Agilent GS-GASPRO, Φ0.32 × 60 m). The concentration of SO<sub>2</sub>, CO<sub>2</sub> or N<sub>2</sub> in the outlet gas was monitored by the TCD. After the



breakthrough experiment, the sample was regenerated with He flow (7 to 15 mL min<sup>-1</sup>) for 6–20 h.

**Density-Functional Theory Calculations:** First-principles density-functional theory (DFT) calculations were performed using the Quantum-Espresso package. A semi-empirical addition of dispersive forces to conventional DFT was included in the calculation to account for van der Waals interactions.<sup>[46]</sup> Vanderbilt-type ultrasoft pseudopotentials and generalized gradient approximation with Perdew–Burke–Ernzerhof exchange correlation were used. A cutoff energy of 544 eV and a 2 × 2 × 4 k-point mesh (generated using the Monkhorst–Pack scheme) were found to be enough for the total energy to converge within 0.01 meV atom<sup>-1</sup>. The structure of SIFSIX MOFs was first optimized. The optimized structures are good matches for the experimentally determined crystal structures of the coordination networks. Various guest gas molecules were then introduced to various locations of the channel pore, followed by a full structural relaxation. To obtain the gas binding energy, an isolated gas molecule placed in a supercell (with the same cell dimensions as the MOF crystal) was also relaxed as a reference. The static binding energy (at T = 0 K) was then calculated using: E<sub>B</sub> = E(MOF) + E(gas) – E(MOF + gas).

**Fitting of Isotherms:** The isotherm data for SO<sub>2</sub>, CO<sub>2</sub>, CH<sub>4</sub>, and N<sub>2</sub> in SIFSIX-1-Cu, SIFSIX-2-Cu-i, SIFSIX-3-Zn, and SIFSIX-3-Ni were fitted with either the Langmuir–Freundlich isotherm model:

$$q = q_{\text{sat}} \frac{bp^v}{1 + bp^v} \quad (1)$$

with T-dependent parameters b:

$$b = b_0 \exp\left(\frac{E}{RT}\right) \quad (2)$$

**IAST Calculations of Adsorption Selectivities:** The adsorption selectivity for C<sub>2</sub>H<sub>2</sub>/C<sub>2</sub>H<sub>4</sub> separation is defined by:

$$S_{\text{ads}} = \frac{q_1/q_2}{p_1/p_2} \quad (3)$$

where q<sub>1</sub> and q<sub>2</sub> are the molar loadings in the adsorbed phase in equilibrium with the bulk gas phase with partial pressures p<sub>1</sub>, and p<sub>2</sub>.

## Supporting Information

Supporting Information is available from the Wiley Online Library or from the author.

## Acknowledgements

This work was supported by the National Natural Science Foundation of China (Grant No. 21436010), National Program for Support of Top-Notch Young Professionals (to H. X.), National Key Research and Development Plan (Grant No. 2016YFB0301500), Zhejiang Provincial Natural Science Foundation of China (Grant No. LR13B060001), and the Welch Foundation (Grant No. AX-1730). The structures of SIFSIX-1-Cu-SO<sub>2</sub> (reference numbers CCDC 1545669) and SIFSIX-2-Cu-i-SO<sub>2</sub> (CCDC 1545670) are available free of charge from the Cambridge Crystallographic Data Centre via www.ccdc.cam.ac.uk/data\_request/cif.

## Conflict of Interest

The authors declare no conflict of interest.

## Keywords

adsorption, gas purification, ionic hybrid porous materials, SO<sub>2</sub> cluster, sulfur dioxide

Received: December 22, 2016

Revised: April 25, 2017

Published online: May 31, 2017

- [1] A. Laurent, N. Espinosa, *Energy Environ. Sci.* **2015**, *8*, 689.
- [2] M. W. Ryberg, M. Owsianiak, A. Laurent, M. Z. Hauschild, *Energy Environ. Sci.* **2015**, *8*, 2435.
- [3] Z. Klimont, S. J. Smith, J. Cofala, *Environ. Res. Lett.* **2013**, *8*, 014003.
- [4] Y. Wang, Q. Q. Zhang, K. He, Q. Zhang, L. Chai, *Atmos. Chem. Phys.* **2013**, *13*, 2635.
- [5] Y. Zhao, L. Duan, J. Xing, T. Larssen, C. P. Nielsen, J. M. Hao, *Environ. Sci. Technol.* **2009**, *43*, 8021.
- [6] Y. Xu, R. H. Williams, R. H. Socolow, *Energy Environ. Sci.* **2009**, *2*, 459.
- [7] R. Pacciani, J. Torres, P. Solsona, C. Coe, R. Quinn, J. Hufton, T. Golden, L. F. Vega, *Environ. Sci. Technol.* **2011**, *45*, 7083.
- [8] R. K. Srivastava, W. Jozewicz, C. Singer, *Environ. Prog.* **2001**, *20*, 219.
- [9] S. Ding, F. Liu, X. Y. Shi, K. Liu, Z. H. Lian, L. J. Xie, H. He, *ACS Appl. Mater. Interfaces* **2015**, *7*, 9497.
- [10] J. S. Valente, R. Quintana-Solorzano, *Energy Environ. Sci.* **2011**, *4*, 4096.
- [11] K. Chen, W. Lin, X. Yu, X. Luo, F. Ding, X. He, H. Li, *AIChE J.* **2015**, *61*, 2028.
- [12] P. Córdoba, *Fuel* **2015**, *144*, 274.
- [13] X. Wang, X. Ma, S. Zhao, B. Wang, C. Song, *Energy Environ. Sci.* **2009**, *2*, 878.
- [14] R. Tailor, M. Abboud, A. Sayari, *Environ. Sci. Technol.* **2014**, *48*, 2025.
- [15] K.-J. Chen, H. S. Scott, D. G. Madden, T. Pham, A. Kumar, A. Bajpai, M. Lusi, K. A. Forrest, B. Space, J. J. Perry IV, M. J. Zaworotko, *Chem* **2016**, *1*, 753.
- [16] P.-Q. Liao, W.-X. Zhang, J.-P. Zhang, X.-M. Chen, *Nat. Commun.* **2015**, *6*, 8697.
- [17] H.-C. Zhou, J. R. Long, O. M. Yaghi, *Chem. Rev.* **2012**, *112*, 673.
- [18] J.-R. Li, J. Sculley, H.-C. Zhou, *Chem. Rev.* **2012**, *112*, 869.
- [19] P. Nugent, Y. Belmabkhout, S. D. Burd, A. J. Cairns, R. Luebke, K. Forrest, T. Pham, S. Q. Ma, B. Space, L. Wojtas, M. Eddaoudi, M. J. Zaworotko, *Nature* **2013**, *495*, 80.
- [20] A. Cadiau, K. Adil, P. M. Bhatt, Y. Belmabkhout, M. Eddaoudi, *Science* **2016**, *353*, 137.
- [21] S. Yang, A. J. Ramirez-Cuesta, R. Newby, V. Garcia-Sakai, P. Manuel, S. K. Callear, S. I. Campbell, C. C. Tang, M. Schroder, *Nat. Chem.* **2015**, *7*, 121.
- [22] T.-L. Hu, H. Wang, B. Li, R. Krishna, H. Wu, W. Zhou, Y. Zhao, Y. Han, X. Wang, W. Zhou, Z. Yao, S. Xiang, B. Chen, *Nat. Commun.* **2015**, *6*, 7328.
- [23] E. D. Bloch, W. L. Queen, R. Krishna, J. M. Zadrozny, C. M. Brown, J. R. Long, *Science* **2012**, *335*, 1606.
- [24] S.-I. Noro, R. Kitaura, M. Kondo, S. Kitagawa, T. Ishii, H. Matsuzaka, M. Yamashita, *J. Am. Chem. Soc.* **2002**, *124*, 2569.
- [25] Z. Bao, G. Chang, H. Xing, R. Krishna, Q. Ren, B. Chen, *Energy Environ. Sci.* **2016**, *9*, 3612.
- [26] W.-Y. Gao, W. Yan, R. Cai, K. Williams, A. Salas, L. Wojtas, X. Shi, S. Ma, *Chem. Commun.* **2012**, *48*, 8898.
- [27] Q.-G. Zhai, X. Bu, C. Mao, X. Zhao, P. Feng, *J. Am. Chem. Soc.* **2016**, *138*, 2524.

- [28] O. M. Farha, A. ö. Yazaydin, I. Eryazici, C. D. Malliakas, B. G. Hauser, M. G. Kanatzidis, S. T. Nguyen, R. Q. Snurr, J. T. Hupp, *Nat. Chem.* **2010**, *2*, 944.
- [29] H. Wang, X.-L. Wang, J. Li, *ChemPlusChem* **2016**, *81*, 872.
- [30] D. Britt, D. Tranchemontagne, O. M. Yaghi, *Proc. Natl. Acad. Sci. USA* **2008**, *105*, 11623.
- [31] T. G. Glover, G. W. Peterson, B. J. Schindler, D. Britt, O. Yaghi, *Chem. Eng. Sci.* **2011**, *66*, 163.
- [32] Z. Arcís-Castillo, F. J. Muñoz-Lara, M. C. Muñoz, D. Aravena, A. B. Gaspar, J. F. Sánchez-Royo, E. Ruiz, M. Ohba, R. Matsuda, S. Kitagawa, J. A. Real, *Inorg. Chem.* **2013**, *52*, 12777.
- [33] S. Yang, L. Liu, J. Sun, K. M. Thomas, A. J. Davies, M. W. George, A. J. Blake, A. H. Hill, A. N. Fitch, C. C. Tang, M. Schröder, *J. Am. Chem. Soc.* **2013**, *135*, 4954.
- [34] S. Yang, J. Sun, A. J. Ramirez-Cuesta, S. K. Callear, W. I. F. David, D. P. Anderson, R. Newby, A. J. Blake, J. E. Parker, C. C. Tang, M. Schröder, *Nat. Chem.* **2012**, *4*, 887.
- [35] M. Savage, Y. Cheng, T. L. Easun, J. E. Eyley, S. P. Argent, M. R. Warren, W. Lewis, C. Murray, C. C. Tang, M. D. Frogley, G. Cinque, J. Sun, S. Rudi, R. T. Murden, M. J. Benham, A. N. Fitch, A. J. Blake, A. J. Ramirez-Cuesta, S. Yang, M. Schröder, *Adv. Mater.* **2016**, *28*, 8705.
- [36] K. Tan, P. Canepa, Q. Gong, J. Liu, D. H. Johnson, A. Dyevoich, P. K. Thallapally, T. Thonhauser, J. Li, Y. J. Chabal, *Chem. Mater.* **2013**, *25*, 4653.
- [37] L. Ding, A. O. Yazaydin, *Phys. Chem. Phys.* **2013**, *15*, 11856.
- [38] J. Yu, Y. Ma, P. B. Balbuena, *Langmuir* **2012**, *28*, 8064.
- [39] X. Cui, K. Chen, H. Xing, Q. Yang, R. Krishna, Z. Bao, H. Wu, W. Zhou, X. Dong, Y. Han, B. Li, Q. Ren, M. J. Zaworotko, B. Chen, *Science* **2016**, *353*, 141.
- [40] L. Wu, D. An, J. Dong, Z. Zhang, B.-G. Li, S. Zhu, *Macromol. Rapid Commun.* **2006**, *27*, 1949.
- [41] H. Yi, Z. Wang, H. Liu, X. Tang, D. Ma, S. Zhao, B. Zhang, F. Gao, Y. Zuo, *J. Chem. Eng. Data* **2014**, *59*, 1556.
- [42] K. S. Walton, D. S. Sholl, *AIChE J.* **2015**, *61*, 2757.
- [43] R. Krishna, *RSC Adv.* **2015**, *5*, 52269.
- [44] M. Alvarez, F. J. Bermejo, P. Chieux, E. Enciso, M. Garcia-Hernandez, N. Garcia, J. Alonso, *Mol. Phys.* **1989**, *66*, 397.
- [45] B. Post, R. S. Schwartz, I. Fankuchen, *Acta Cryst.* **1952**, *5*, 372.
- [46] V. Barone, M. Casarin, D. Forrer, M. Pavone, M. Sambì, A. Vittadini, *Comput. Chem.* **2009**, *30*, 934.

# ADVANCED MATERIALS

## Supporting Information

for *Adv. Mater.*, DOI: 10.1002/adma.201606929

Ultrahigh and Selective SO<sub>2</sub> Uptake in Inorganic Anion-Pillared Hybrid Porous Materials

*Xili Cui, Qiwei Yang,\* Lifeng Yang, Rajamani Krishna, Zhiguo Zhang, Zongbi Bao, Hui Wu, Qilong Ren, Wei Zhou, Banglin Chen,\* and Huabin Xing\**

## Supporting Information

**Ultrahigh and Selective SO<sub>2</sub> Uptake in Inorganic Anion-Pillared Hybrid Porous Materials**

*Xili Cui, Qiwei Yang,\* Lifeng Yang, Rajamani Krishna, Zhiguo Zhang, Zongbi Bao, Hui Wu, Qilong Ren, Wei Zhou, Banglin Chen,\* Huabin Xing\**

Dr. X. L. Cui, Dr. Q. W. Yang, L. F. Yang, Dr. Z. G. Zhang, Dr. Z. B. Bao, Prof. Q. L. Ren, Prof. H. B. Xing

Key Laboratory of Biomass Chemical Engineering of Ministry of Education, College of Chemical and Biological Engineering, Zhejiang University, Hangzhou 310027, China

E-mail: [xinghb@zju.edu.cn](mailto:xinghb@zju.edu.cn) [yangqw@zju.edu.cn](mailto:yangqw@zju.edu.cn)

Prof. R. Krishna

Van' t Hoff Institute for Molecular Sciences, University of Amsterdam, Science Park 904, 1098 XH Amsterdam, Netherlands

Dr. H. Wu, Prof. W. Zhou

Center for Neutron Research, National Institute of Standards and Technology, Gaithersburg, Maryland 20899-6102, USA.

Prof. B. L. Chen

Department of Chemistry, University of Texas at San Antonio, One UTSA Circle, San Antonio, Texas 78249-0698, USA

E-mail: [Banglin.Chen@utsa.edu](mailto:Banglin.Chen@utsa.edu)

**This PDF file includes:**

Materials and Methods

Tables S1-S6

Figures. S3 to S18

## Experiments

### *Materials*

Ammonium hexafluorosilicate ((NH)<sub>2</sub>SiF<sub>6</sub>, 98%, Aldrich), copper (II) tetrafluoroborate hydrate (Cu(BF<sub>4</sub>)<sub>2</sub>• xH<sub>2</sub>O, 98%, Aldrich), zinc hexafluorosilicate hydrate (ZnSiF<sub>6</sub>• xH<sub>2</sub>O, 99%, Aldrich), 4,4'-bipyridine (C<sub>10</sub>H<sub>8</sub>N<sub>2</sub>, 98%, Aldrich), 4-(2-pyridin-4-ylethynyl)pyridine (C<sub>12</sub>H<sub>8</sub>N<sub>2</sub>, 98%, Chemsoon), pyrazine (C<sub>4</sub>H<sub>4</sub>N<sub>2</sub>, 99%, Aldrich), methanol (CH<sub>3</sub>OH, anhydrous, 99%, Sigma-Aldrich), ethylene glycol (C<sub>2</sub>H<sub>6</sub>O<sub>2</sub>, anhydrous, 99%, Sigma-Aldrich), were purchased and used without further purification.

N<sub>2</sub> (99.999%), CO<sub>2</sub> (99%), CH<sub>4</sub> (99.99%), He (99.999%), SO<sub>2</sub> (99.99%) and mixed gases of (1) SO<sub>2</sub>/N<sub>2</sub> = 0.2/99.8 (v/v), (2) SO<sub>2</sub>/N<sub>2</sub> = 1/99 (v/v), (3) SO<sub>2</sub>/N<sub>2</sub> = 5/95 (v/v), (4) SO<sub>2</sub>/N<sub>2</sub> = 10/90 (v/v) were purchased from JinGong Company (China). Mixed gases of (5) SO<sub>2</sub>/CO<sub>2</sub> = 0.2/99.8 (v/v) were purchased from Shanghai Wetry Standard Reference Gas Analytical Technology Co. LTD (China).

### *Synthesis*

Synthesis of SIFSIX-1-Cu (Cu(4,4'-bipyridine)<sub>2</sub>SiF<sub>6</sub>•8H<sub>2</sub>O)<sub>n</sub>

Firstly, 4,4'-bipyridine (0.35 g) was dissolved in ethylene glycol (40 mL) at 338 K. An aqueous solution (20 mL) of Cu(BF<sub>4</sub>)<sub>2</sub>•xH<sub>2</sub>O (266 mg, 1.12 mmol) and (NH<sub>4</sub>)<sub>2</sub>SiF<sub>6</sub> (199 mg, 1.12 mmol) was added to the above solution. Then the mixture was heated at 65 °C for 3 h under stirring. The obtained purple powder was filtered, washed with methanol, and was exchanged with methanol for 3 days.<sup>[1]</sup>

Synthesis of SIFSIX-2-Cu (Cu(4,4'-bipyridylacetylene)<sub>2</sub>SiF<sub>6</sub>)<sub>n</sub>

An ethanol solution (2.0 mL) of 4,4'-bipyridylacetylene (0.115mmol) was carefully layered onto an ethylene glycol solution (2.0 mL) of CuSiF<sub>6</sub>•xH<sub>2</sub>O (0.149 mmol). Crystals of SIFSIX-2-Cu were obtained after two weeks. The obtained sample was exchanged with ethanol for 4 days.<sup>[2]</sup>

Synthesis of SIFSIX-2-Cu-i (Cu(4,4'-bipyridylacetylene)<sub>2</sub>SiF<sub>6</sub>).

A methanol solution (4.0 mL) of 4,4'-bipyridylacetylene (0.286 mmol) was mixed with an aqueous solution (4.0 mL) of  $\text{Cu}(\text{BF}_4)_2 \cdot x\text{H}_2\text{O}$  (0.26 mmol) and  $(\text{NH}_4)_2\text{SiF}_6$  (0.26 mmol) and then heated at 85 °C for 12 h. The obtained sample was exchanged with methanol for 3 days.

[2]

Synthesis of SIFSIX-3-Zn ( $\text{Zn}(\text{pyrazine})_2\text{SiF}_6$ )<sub>n</sub>

A methanol solution (2.0 mL) of pyrazine (1.3 mmol) was carefully layered onto a methanol solution (2.0 mL) of  $\text{ZnSiF}_6 \cdot x\text{H}_2\text{O}$  (0.13 mmol). Colourless crystals of SIFSIX-3-Zn were obtained after two days. The obtained sample was exchanged with ethanol for 1 days. [2]

Synthesis of SIFSIX-3-Ni ( $\text{Ni}(\text{pyrazine})_2\text{SiF}_6$ )<sub>n</sub>

A methanol solution (20 ml) of nickel silicofluoride,  $\text{NiSiF}_6$  (1 mmol) and pyrazine (2 mmol) was mixed and heated at 85 °C. Blue powder was obtained after 3 days. The obtained sample was exchanged with ethanol for 3 days. [3]

### ***Pure gas adsorption***

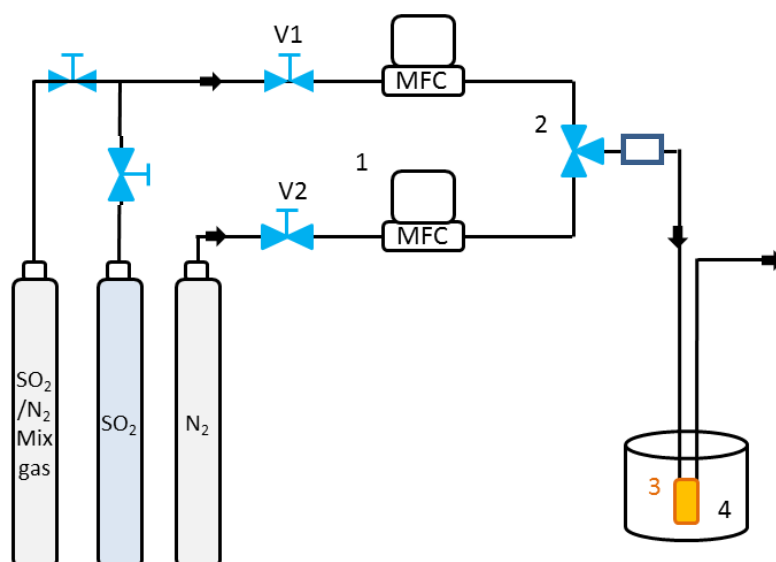
SIFSIX-1-Cu, SIFSIX-2-Cu, SIFSIX-2-Cu-i, and SIFSIX-3-Zn were evacuated at 303 K for 1-2 days until the pressure dropped below 7 μm Hg. SIFSIX-3-Ni was degased at 105 °C for 15 h under dynamic pressure below 5 μm Hg.  $\text{N}_2$ ,  $\text{CO}_2$  and  $\text{CH}_4$  sorption isotherms were collected at 298 K on activated SIFSIX-1-Cu, SIFSIX-2-Cu, SIFSIX-2-Cu-i, SIFSIX-3-Ni and SIFSIX-3-Zn using ASAP 2050 Analyzer (Micromeritics).

### ***SO<sub>2</sub> adsorption***

$\text{SO}_2$  adsorption isotherms at 298 K and 273 K were collected using the apparatus in Figure S1. Activated samples were packed in a glass container which was partly immersed in a water bath. The  $\text{SO}_2$  adsorption isotherms were determined using  $\text{SO}_2/\text{N}_2$  mixed gas with varying  $\text{SO}_2$  molar fractions under flow mode. Note: the adsorption of  $\text{SO}_2$  at 1.0 atm was measured with pure  $\text{SO}_2$  at flow mode. At the beginning of this experiment, the activated sample was loaded in the glass container which was full of pure  $\text{N}_2$  atmosphere at 760 mmHg. Then the  $\text{SO}_2/\text{N}_2$  mixed gas (e.g. 0.002/99.998) was introduced at a constant flow at 760 mmHg.

Adsorption equilibrium was reached until the weight of glass container kept constant and didn't change. The  $\text{SO}_2$  uptake was calculated based on the weight-change before and after dynamic adsorption. This method will underestimate the  $\text{SO}_2$  uptake because the samples were pre-saturated by  $\text{N}_2$  but some of  $\text{N}_2$  molecules were displaced by the  $\text{SO}_2$  molecules. At the adsorption with high  $\text{SO}_2$  molar fraction, the weight of unadsorbed  $\text{SO}_2$  gases in the glass container was subtracted by blank test.

The detailed adsorption procedures: firstly,  $\text{SO}_2/\text{N}_2$  (0.002/0.998) mixed gas was introduced into the glass container at a rate of  $20 \text{ ml min}^{-1}$ . Equilibrium were reached until the weight of glass container kept constant and didn't change. The amount of adsorbed  $\text{SO}_2$  at the partial pressure of 0.002 was determined by the electronic balance with  $\pm 0.1 \text{ mg}$  accuracy. Then, the uptake capacity of  $\text{SO}_2$  at the partial pressure of 0.01, 0.05, 0.1 was measured using  $\text{SO}_2/\text{N}_2$  (0.01/0.99),  $\text{SO}_2/\text{N}_2$  (0.05/0.95),  $\text{SO}_2/\text{N}_2$  (0.1/0.9) mixed gas using the repeated procedures. The higher partial pressure of  $\text{SO}_2$  (e.g. 0.4, 0.5, 0.8 1.0) was controlled by changing the flow rate of  $\text{SO}_2$  and  $\text{N}_2$ .



1. Mass flow controller    2. 3-Way valve    3. Glass container    4. Water bath

**Figure S1** Schematic illustration of the apparatus for the  $\text{SO}_2$  adsorption experiments.

**Breakthrough tests**

The breakthrough experiments were carried out in a dynamic gas breakthrough equipment (fig. S2).<sup>[4]</sup> All experiments were conducted using a stainless steel column (4.6 mm inner diameter  $\times$  50 mm). According to the different particle size and density of the sample powder, the weight packed in the column was: SIFSIX-1-Cu powder (0.21 g), SIFSIX-2-Cu-i (0.21 g), and SIFSIX-3-Ni (0.50 g), respectively. The column packed with sample was firstly purged with He flow (15 ml min<sup>-1</sup>) for 12 h at room temperature (25 °C). The mixed gas of SO<sub>2</sub>/N<sub>2</sub> = 0.2/99.8 (v/v) was then introduced at 21 ml min<sup>-1</sup>, and SO<sub>2</sub>/CO<sub>2</sub> = 0.2/99.8 (v/v) was introduced at 14 ml min<sup>-1</sup>. Outlet gas from the column was monitored using gas chromatography (GC-2010 plus) with a thermal conductivity detector (TCD) coupled with a FID. The gas mixture was separated by a capillary column (Agilent GS-GASPRO,  $\Phi$ 0.32  $\times$  60 M). The concentration of SO<sub>2</sub>, CO<sub>2</sub> or N<sub>2</sub> in the outlet gas was monitored by the TCD. After the breakthrough experiment, the sample was regenerated with He flow (7 to 15 ml min<sup>-1</sup>) for 6 to 20 hours.

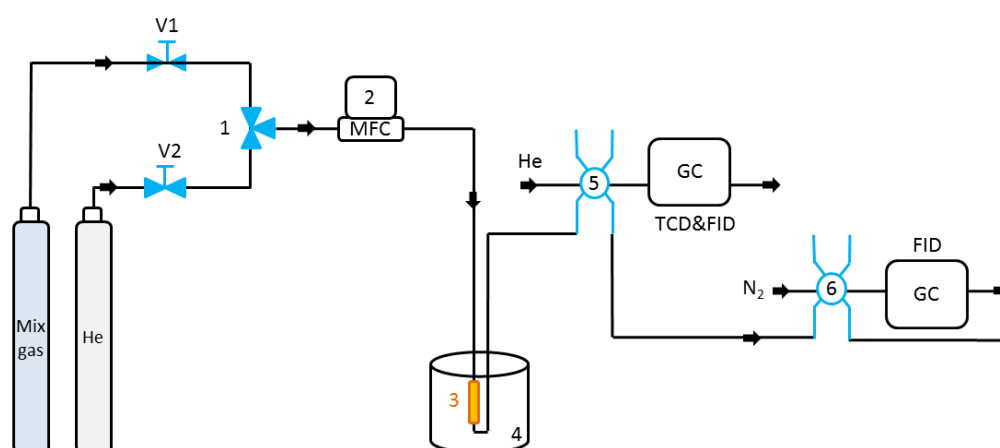


**Figure S2** Schematic illustration of the apparatus for the breakthrough experiments.



### *X-ray diffraction structure analysis*

Powder X-ray diffraction patterns were collected using SHIMADZU XRD-6000 diffractometer (Cu  $K_{\alpha}$   $\lambda = 1.540598 \text{ \AA}$ ) with an operating power of 40 Kv and fixed divergence slit of 0.76 mm. The data were collected in the range of  $2\theta = 3-50^{\circ}$ .

Powder X-ray diffraction patterns of bare and SO<sub>2</sub>-loaded SIFSIX-1-Cu and SIFSIX-2-Cu-i were collected using PANalytical X'Pert Pro diffractometer (Cu  $K_{\alpha}$   $\lambda = 1.540598 \text{ \AA}$ ) with an operating power of 40 Kv and fixed divergence slit of 0.380 mm. The data were collected in the range of  $2\theta = 3-60^{\circ}$ .

### *Density-functional theory calculations*

First-principles density-functional theory (DFT) calculations were performed using the Quantum-Espresso package. A semi-empirical addition of dispersive forces to conventional DFT was included in the calculation to account for van der Waals interactions.<sup>[5]</sup> We used Vanderbilt-type ultrasoft pseudopotentials and generalized gradient approximation (GGA) with Perdew-Burke-Ernzerhof (PBE) exchange correlation. A cutoff energy of 544 eV and a  $2 \times 2 \times 4$  k-point mesh (generated using the Monkhorst-Pack scheme) were found to be enough for the total energy to converge within 0.01 meV atom<sup>-1</sup>. We first optimized the structure of SIFSIX MOFs. The optimized structures are good matches for the experimentally determined crystal structures of the coordination networks. Various guest gas molecules were then introduced to various locations of the channel pore, followed by a full structural relaxation. To obtain the gas binding energy, an isolated gas molecule placed in a supercell (with the same cell dimensions as the MOF crystal) was also relaxed as a reference. The static binding energy (at  $T = 0 \text{ K}$ ) was then calculated using:  $EB = E(\text{MOF}) + E(\text{gas}) - E(\text{MOF}+\text{gas})$ .

### *Fitting of isotherms*

The isotherm data for SO<sub>2</sub>, CO<sub>2</sub>, CH<sub>4</sub>, and N<sub>2</sub> in SIFSIX-1-Cu, SIFSIX-2-Cu-i, SIFSIX-3-Zn, and SIFSIX-3-Ni were fitted with either the Langmuir-Freundlich isotherm model.

$$q = q_{sat} \frac{bp^\nu}{1 + bp^\nu} \quad (1)$$

with  $T$ -dependent parameters  $b$

$$b = b_0 \exp\left(\frac{E}{RT}\right) \quad (2)$$

The fitted parameter values are presented in Table S1

Notation

|           |   |
|-----------|---|
| $b$       | Langmuir-Freundlich constant, $\text{Pa}^{-\nu}$        |
| $E$       | energy parameter, $\text{J mol}^{-1}$                   |
| $p$       | pressure, Pa  |
| $q$       | component molar loading, $\text{mol kg}^{-1}$           |
| $q_{sat}$ | saturation loading, $\text{mol kg}^{-1}$                |
| $R$       | gas constant, $8.314 \text{ J mol}^{-1} \text{ K}^{-1}$ |
| $T$       | absolute temperature, K                                 |

### ***Isosteric heat of adsorption***

The binding energy of  $\text{SO}_2$  is reflected in the isosteric heat of adsorption,  $Q_{st}$ , defined as

$$Q_{st} = RT^2 \left( \frac{\partial \ln p}{\partial T} \right)_q \quad (3)$$

Figure S3 presents a comparison of the heats of adsorption of  $\text{SO}_2$  in various SIFSIX; the calculations are based on the use of the Clausius-Clapeyron equation.

### ***IAST calculations of adsorption selectivities***

The adsorption selectivity for  $\text{C}_2\text{H}_2/\text{C}_2\text{H}_4$  separation is defined by

$$S_{ads} = \frac{q_1/q_2}{p_1/p_2} \quad (3)$$

$q_1$ , and  $q_2$  are the molar loadings in the adsorbed phase in equilibrium with the bulk gas phase with partial pressures  $p_1$ , and  $p_2$ .

**Table S1.** Langmuir-Freundlich parameter fits for SO<sub>2</sub>, CO<sub>2</sub>, CH<sub>4</sub>, and N<sub>2</sub> in SIFSIX materials. The isotherm data for CH<sub>4</sub>, and N<sub>2</sub> were only measured at 298 K, and therefore  $E = 0$ .

| SIFSIX-1-Cu     |  |  |                             |                        |
|-----------------|--|--|-----------------------------|------------------------|
|                 | $q_{\text{sat}}$<br>mol kg <sup>-1</sup> | $b_0$<br>Pa <sup>-<math>\nu_i</math></sup> | $E$<br>kJ mol <sup>-1</sup> | $\nu$<br>dimensionless |
| SO <sub>2</sub> | 11.7                                     | $9.8 \times 10^{-8}$                       | 26                          | 0.72                   |
| CO <sub>2</sub> | 12                                       | $1.12 \times 10^{-13}$                     | 33                          | 1.2                    |
| CH <sub>4</sub> | 12                                       | $3.9 \times 10^{-7}$                       | 0                           | 1                      |
| N <sub>2</sub>  | 12                                       | $1.54 \times 10^{-7}$                      | 0                           | 1                      |

| SIFSIX-2-Cu-i   |  |  |                             |                        |
|-----------------|--|--|-----------------------------|------------------------|
|                 | $q_{\text{sat}}$<br>mol kg <sup>-1</sup> | $b_0$<br>Pa <sup>-<math>\nu_i</math></sup> | $E$<br>kJ mol <sup>-1</sup> | $\nu$<br>dimensionless |
| SO <sub>2</sub> | 7.1                                      | $1.33 \times 10^{-6}$                      | 23.6                        | 0.62                   |
| CO <sub>2</sub> | 6.5                                      | $4.9 \times 10^{-11}$                      | 33                          | 1                      |
| CH <sub>4</sub> | 12                                       | $4.87 \times 10^{-7}$                      | 0                           | 1                      |
| N <sub>2</sub>  | 12                                       | $1.6 \times 10^{-7}$                       | 0                           | 1                      |

| SIFSIX-3-Ni     |  |  |                             |                        |
|-----------------|--|--|-----------------------------|------------------------|
|                 | $q_{\text{sat}}$<br>mol kg <sup>-1</sup> | $b_0$<br>Pa <sup>-<math>\nu_i</math></sup> | $E$<br>kJ mol <sup>-1</sup> | $\nu$<br>dimensionless |
| SO <sub>2</sub> | 2.7                                      | $3.05 \times 10^{-11}$                     | 46.2                        | 1.07                   |
| CH <sub>4</sub> | 12                                       | $3.9 \times 10^{-7}$                       | 0                           | 1                      |
| N <sub>2</sub>  | 12                                       | $2.08 \times 10^{-7}$                      | 0                           | 1                      |

| SIFSIX-3-Zn     |  |  |                             |                        |
|-----------------|--|--|-----------------------------|------------------------|
|                 | $q_{\text{sat}}$<br>mol kg <sup>-1</sup> | $b_0$<br>Pa <sup>-<math>\nu_i</math></sup> | $E$<br>kJ mol <sup>-1</sup> | $\nu$<br>dimensionless |
| SO <sub>2</sub> | 2.25                                     | $4.1 \times 10^{-6}$                       | 23.5                        | 0.52                   |
| CH <sub>4</sub> | 12                                       | $3.78 \times 10^{-7}$                      | 0                           | 1                      |
| N <sub>2</sub>  | 12                                       | $2.08 \times 10^{-7}$                      | 0                           | 1                      |

**Table S2.** The volumetric uptake of SO<sub>2</sub> (density per crystal cell volume) in various SIFSIX materials at 1.01 bar.

|               | Framework density<br>(g cm <sup>-3</sup> ) | C <sub>2</sub> H <sub>2</sub> density per crystal cell volume (g cm <sup>-3</sup> ) |                |
|---------------|--|---|----------------|
|               |  | 298 K   | 283 K<br>273 K |
| SIFSIX-1-Cu   | 0.864                                      | 0.609   | 0.658          |
| SIFSIX-2-Cu-i | 1.247                                      | 0.551   | 0.575          |
| SIFSIX-3-Zn   | 1.574                                      | 0.212   | 0.237          |
| SIFSIX-3-Ni   | 1.610                                      | 0.282   | 0.299          |

**Table S3.** List of atomic positions for SIFSIX-1-Cu·SO<sub>2</sub>

| Atom | a       | b       | c       |
|------|---------|---------|---------|
| N6   | 0.00000 | 0.18296 | 0.00000 |
| C5   | 0.00000 | 0.43393 | 0.00000 |
| C1   | 0.03427 | 0.24303 | 0.13464 |
| C2   | 0.03491 | 0.36849 | 0.13817 |
| H3   | 0.06405 | 0.19281 | 0.24102 |
| H4   | 0.06545 | 0.41511 | 0.24710 |
| Cu7  | 0.00000 | 0.00000 | 0.00000 |
| Si8  | 0.00000 | 0.00000 | 0.50000 |
| F9   | 0.00000 | 0.00000 | 0.28490 |
| F10  | 0.10630 | 0.10630 | 0.50000 |
| S11  | 0.28855 | 0.30438 | 0.56560 |
| O12  | 0.40425 | 0.26932 | 0.49696 |
| O13  | 0.21666 | 0.39012 | 0.47061 |

| Unit cell parameters |  |
|----------------------|--|
| Formula sum          | N C3 H2 Cu Si F2 S0.252 O0.503                                   |
| Formula weight       | 197.81 g mol <sup>-1</sup>                                       |
| Space-group          | P 422  |
| Cell parameters      | a=11.1348 Å b=11.1348 Å c=8.0047 Å α=90.00°<br>β=90.00° γ=90.00° |
| Cell ratio           | a/b=1.0000 b/c=1.3910 c/a=0.7189                                 |
| Cell volume          | 992.47 Å <sup>3</sup>  |

**Table S4.** List of Miller Index of the simulated pattern of SIFSIX-1-Cu•SO<sub>2</sub>

| 2 Theta | h | k | l | d-spacing |
|---------|---|---|---|-----------|
| 7.934   | 1 | 0 | 0 | 11.1348   |
| 11.044  | 0 | 0 | 1 | 8.00474   |
| 11.229  | 1 | 1 | 0 | 7.87352   |
| 13.613  | 1 | 0 | 1 | 6.49954   |
| 15.775  | 1 | 1 | 1 | 5.61324   |
| 15.906  | 2 | 0 | 0 | 5.56742   |
| 17.798  | 2 | 1 | 0 | 4.97965   |
| 19.406  | 2 | 0 | 1 | 4.57062   |
| 20.993  | 2 | 1 | 1 | 4.22826   |
| 22.193  | 0 | 0 | 2 | 4.00237   |
| 22.568  | 2 | 2 | 0 | 3.93676   |
| 22.602  | 1 | 0 | 2 | 3.76645   |
| 23.956  | 3 | 0 | 0 | 3.71162   |
| 24.937  | 1 | 1 | 2 | 3.56786   |
| 25.189  | 2 | 2 | 1 | 3.53265   |
| 25.273  | 3 | 1 | 0 | 3.52115   |
| 26.448  | 3 | 0 | 1 | 3.36725   |
| 27.423  | 2 | 0 | 2 | 3.24977   |
| 27.654  | 3 | 1 | 1 | 3.2231    |
| 28.591  | 2 | 1 | 2 | 3.11962   |
| 28.887  | 3 | 2 | 0 | 3.08825   |
| 31.013  | 3 | 2 | 1 | 2.88126   |
| 31.859  | 2 | 2 | 2 | 2.80662   |
| 32.129  | 4 | 0 | 0 | 2.78371   |
| 32.884  | 3 | 0 | 2 | 2.7215    |
| 33.146  | 4 | 1 | 0 | 2.7006    |
| 33.559  | 0 | 0 | 3 | 2.66825   |
| 33.880  | 3 | 1 | 2 | 2.64368   |
| 34.072  | 4 | 0 | 1 | 2.62926   |
| 34.136  | 3 | 3 | 0 | 2.62451   |
| 34.539  | 1 | 0 | 3 | 2.59479   |
| 35.039  | 4 | 1 | 1 | 2.55889   |
| 35.494  | 1 | 1 | 3 | 2.52708   |
| 35.983  | 3 | 3 | 1 | 2.49389   |
| 36.044  | 4 | 2 | 0 | 2.48983   |
| 36.728  | 3 | 2 | 2 | 2.44501   |
| 37.342  | 2 | 0 | 3 | 2.40618   |
| 37.810  | 4 | 2 | 1 | 2.37747   |
| 38.237  | 2 | 1 | 3 | 2.35189   |
| 39.396  | 4 | 0 | 2 | 2.28531   |
| 40.253  | 4 | 1 | 2 | 2.23865   |
| 40.473  | 5 | 0 | 0 | 2.22697   |
| 40.473  | 4 | 3 | 0 | 2.22697   |
| 40.822  | 2 | 2 | 3 | 2.20873   |
| 41.094  | 3 | 3 | 2 | 2.19473   |
| 41.311  | 5 | 1 | 0 | 2.18372   |
| 41.654  | 3 | 0 | 3 | 2.16651   |

|        |   |   |   |         |
|--------|---|---|---|---------|
| 42.082 | 5 | 0 | 1 | 2.14549 |
| 42.082 | 4 | 3 | 1 | 2.14549 |
| 42.473 | 3 | 1 | 3 | 2.12663 |
| 42.736 | 4 | 2 | 2 | 2.11413 |
| 42.894 | 5 | 1 | 1 | 2.10674 |
| 43.745 | 5 | 2 | 0 | 2.06769 |
| 44.856 | 3 | 2 | 3 | 2.01903 |
| 42.259 | 5 | 2 | 1 | 2.00198 |
| 45.278 | 0 | 0 | 4 | 2.00119 |
| 46.045 | 1 | 0 | 4 | 1.96963 |
| 46.075 | 4 | 4 | 0 | 1.96838 |
| 46.636 | 4 | 3 | 2 | 1.94601 |
| 46.636 | 5 | 0 | 2 | 1.94601 |
| 46.802 | 1 | 1 | 4 | 1.93952 |
| 47.143 | 4 | 0 | 3 | 1.92626 |
| 47.386 | 5 | 1 | 2 | 1.91696 |
| 47.531 | 4 | 4 | 1 | 1.91144 |
| 47.579 | 5 | 3 | 0 | 1.90961 |
| 47.887 | 4 | 1 | 3 | 1.89807 |
| 48.288 | 2 | 0 | 4 | 1.88322 |
| 48.622 | 3 | 3 | 3 | 1.87108 |
| 49.001 | 5 | 3 | 1 | 1.85749 |
| 49.019 | 2 | 1 | 4 | 1.85685 |
| 49.048 | 6 | 0 | 0 | 1.85581 |
| 49.583 | 5 | 2 | 2 | 1.83703 |
| 49.770 | 6 | 1 | 0 | 1.83056 |
| 50.068 | 4 | 2 | 3 | 1.82038 |
| 50.439 | 6 | 0 | 1 | 1.80786 |
| 51.146 | 6 | 1 | 1 | 1.78449 |
| 51.164 | 2 | 2 | 4 | 1.78393 |
| 51.711 | 4 | 4 | 2 | 1.76633 |
| 51.864 | 3 | 0 | 4 | 1.76147 |
| 51.893 | 6 | 2 | 0 | 1.76057 |
| 52.558 | 3 | 1 | 4 | 1.73983 |
| 52.586 | 5 | 4 | 0 | 1.73897 |
| 53.095 | 5 | 3 | 2 | 1.72349 |
| 53.229 | 6 | 2 | 1 | 1.71948 |
| 53.557 | 4 | 3 | 3 | 1.70972 |
| 53.557 | 5 | 0 | 3 | 1.70972 |
| 53.911 | 5 | 4 | 1 | 1.69933 |
| 54.236 | 5 | 1 | 3 | 1.68992 |
| 54.455 | 6 | 0 | 2 | 1.68363 |
| 54.603 | 3 | 2 | 4 | 1.67941 |

---



**Table S5.** List of atomic positions for SIFSIX-2-Cu-i•SO<sub>2</sub>

| Atom | a       | b       | c       |
|------|---------|---------|---------|
| N7   | 0.00000 | 0.14897 | 0.00000 |
| C5   | 0.00000 | 0.64726 | 0.00000 |
| C1   | 0.02267 | 0.19911 | 0.13599 |
| C2   | 0.02503 | 0.30009 | 0.14229 |
| H3   | 0.03526 | 0.15749 | 0.24709 |
| H4   | 0.03655 | 0.33606 | 0.25900 |
| C6   | 0.00000 | 0.54419 | 0.00000 |
| Cu8  | 0.00000 | 0.00000 | 0.00000 |
| Si9  | 0.00000 | 0.00000 | 0.50000 |
| F10  | 0.00000 | 0.00000 | 0.28300 |
| F11  | 0.08780 | 0.08780 | 0.50000 |
| S7   | 0.19765 | 0.22777 | 0.57535 |
| O5   | 0.26019 | 0.19711 | 0.44227 |
| O6   | 0.12431 | 0.30126 | 0.53996 |

| Unit cell parameters |                                  |
|----------------------|----------------------------------|
| Formula sum          | N C3 H Cu Si F2 S0.17 O0.341     |
| Formula weight       | 191.591 g mol <sup>-1</sup>      |
| Space-group          | I 4/ m m m                       |
| Cell parameters      | a=13.7315 Å c=8.2100 Å           |
| Cell ratio           | a/b=1.0000 b/c=1.6725 c/a=0.5979 |
| Cell volume          | 1548.04 Å <sup>3</sup>           |

**Table S6.** List of Miller Index of the simulated pattern of SIFSIX-2-Cu-i•SO<sub>2</sub>

| 2 Theta | h | k | l | d-spacing |
|---------|---|---|---|-----------|
| 9.101   | 1 | 1 | 0 | 9.70963   |
| 12.552  | 1 | 0 | 1 | 7.04657   |
| 12.884  | 2 | 0 | 0 | 6.86575   |
| 18.024  | 2 | 1 | 1 | 4.9175    |
| 18.259  | 2 | 2 | 0 | 4.85482   |
| 20.436  | 3 | 1 | 0 | 4.34228   |
| 21.631  | 0 | 0 | 2 | 4.10502   |
| 22.218  | 3 | 0 | 1 | 3.99784   |
| 23.510  | 1 | 1 | 2 | 3.78099   |
| 25.257  | 2 | 0 | 2 | 3.52329   |
| 25.766  | 3 | 2 | 1 | 3.45482   |
| 25.934  | 4 | 0 | 0 | 3.43287   |
| 27.537  | 3 | 3 | 0 | 3.23654   |
| 28.451  | 2 | 2 | 2 | 3.13464   |
| 28.908  | 4 | 1 | 1 | 3.08613   |
| 29.059  | 4 | 2 | 0 | 3.07046   |
| 29.930  | 3 | 1 | 2 | 2.98304   |
| 33.242  | 5 | 1 | 0 | 2.69297   |
| 33.358  | 1 | 0 | 3 | 2.6839    |
| 34.017  | 4 | 0 | 2 | 2.63341   |
| 34.407  | 4 | 3 | 1 | 2.60445   |
| 34.407  | 5 | 0 | 1 | 2.60445   |
| 35.285  | 3 | 3 | 2 | 2.54159   |
| 35.897  | 2 | 1 | 3 | 2.49969   |
| 36.515  | 4 | 2 | 2 | 2.45875   |
| 36.882  | 5 | 2 | 1 | 2.43513   |
| 37.004  | 4 | 4 | 0 | 2.42741   |
| 38.186  | 5 | 3 | 0 | 2.35493   |
| 38.288  | 3 | 0 | 3 | 2.34886   |
| 39.338  | 6 | 0 | 0 | 2.28858   |
| 40.010  | 5 | 1 | 2 | 2.25169   |
| 40.560  | 3 | 2 | 3 | 2.2224    |
| 41.451  | 6 | 1 | 1 | 2.17666   |
| 41.561  | 6 | 2 | 0 | 2.17114   |
| 42.731  | 4 | 1 | 3 | 2.11439   |
| 43.266  | 4 | 4 | 2 | 2.08944   |
| 43.585  | 5 | 4 | 1 | 2.07488   |
| 44.085  | 0 | 0 | 4 | 2.05251   |
| 44.309  | 5 | 3 | 2 | 2.04268   |
| 45.112  | 1 | 1 | 4 | 2.00813   |
| 45.332  | 6 | 0 | 2 | 1.99892   |
| 45.639  | 6 | 3 | 1 | 1.98617   |
| 46.122  | 2 | 0 | 4 | 1.96652   |
| 46.740  | 7 | 1 | 0 | 1.94193   |
| 46.740  | 5 | 5 | 0 | 1.94193   |
| 46.827  | 4 | 3 | 3 | 1.93852   |
| 46.827  | 5 | 0 | 3 | 1.93852   |

# WILEY-VCH

|        |   |   |   |         |
|--------|---|---|---|---------|
| 47.326 | 6 | 2 | 2 | 1.91923 |
| 47.624 | 7 | 0 | 1 | 1.90794 |
| 47.723 | 6 | 4 | 0 | 1.90422 |
| 48.091 | 2 | 2 | 4 | 1.8905  |
| 48.774 | 5 | 2 | 3 | 1.86558 |
| 49.053 | 3 | 1 | 4 | 1.85565 |
| 49.547 | 7 | 2 | 1 | 1.83828 |
| 50.583 | 7 | 3 | 0 | 1.80303 |
| 51.859 | 4 | 0 | 4 | 1.76164 |
| 52.056 | 7 | 1 | 2 | 1.75542 |
| 52.056 | 5 | 5 | 2 | 1.75542 |
| 52.506 | 6 | 1 | 3 | 1.74143 |
| 52.770 | 3 | 3 | 4 | 1.73335 |
| 52.965 | 6 | 4 | 2 | 1.72741 |
| 53.240 | 6 | 5 | 1 | 1.71916 |
| 53.331 | 8 | 0 | 0 | 1.71644 |
| 53.670 | 4 | 2 | 4 | 1.70637 |
| 54.303 | 5 | 4 | 3 | 1.68798 |

---

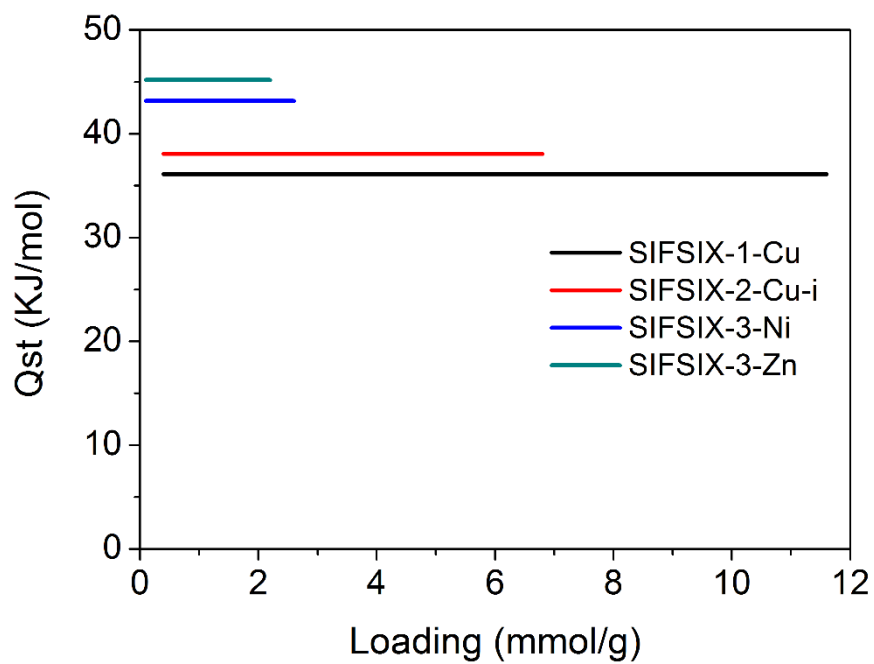


**Figure S3** Comparison of  $Q_{st}$  of  $SO_2$  adsorption in SIFSIX materials.

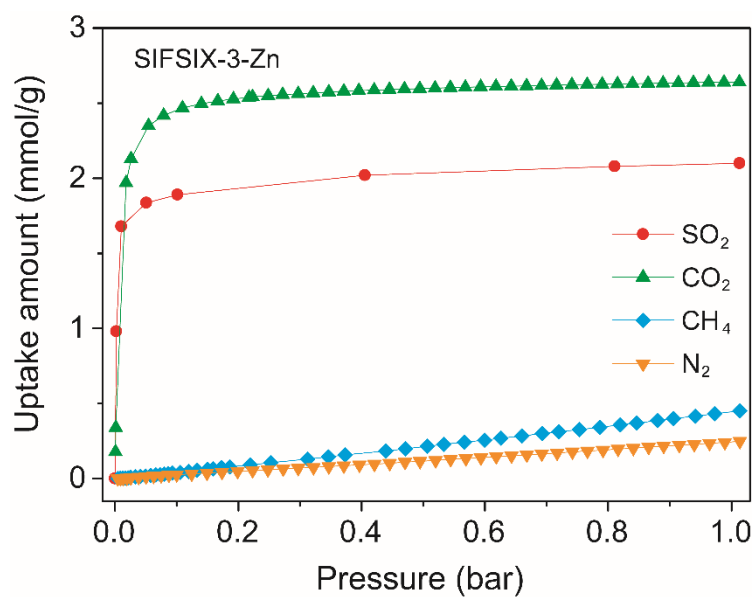


**Figure S4** Adsorption isotherms for SO<sub>2</sub>, CO<sub>2</sub> and CH<sub>4</sub> on SIFSIX-3-Zn at 298 K and 1.0 bar.

Note: the adsorption isotherm of SO<sub>2</sub> were determined using SO<sub>2</sub>/N<sub>2</sub> mixed gas with varying SO<sub>2</sub> molar fractions under flow mode.

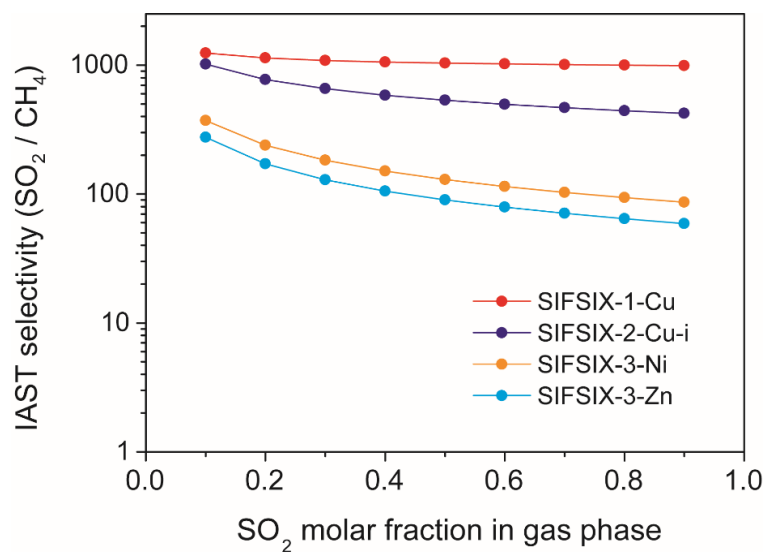


**Figure S5** IAST selectivities of SO<sub>2</sub>/CH<sub>4</sub> on SIFSIX materials with varying SO<sub>2</sub> molar fractions in gas phase at 100 kPa.

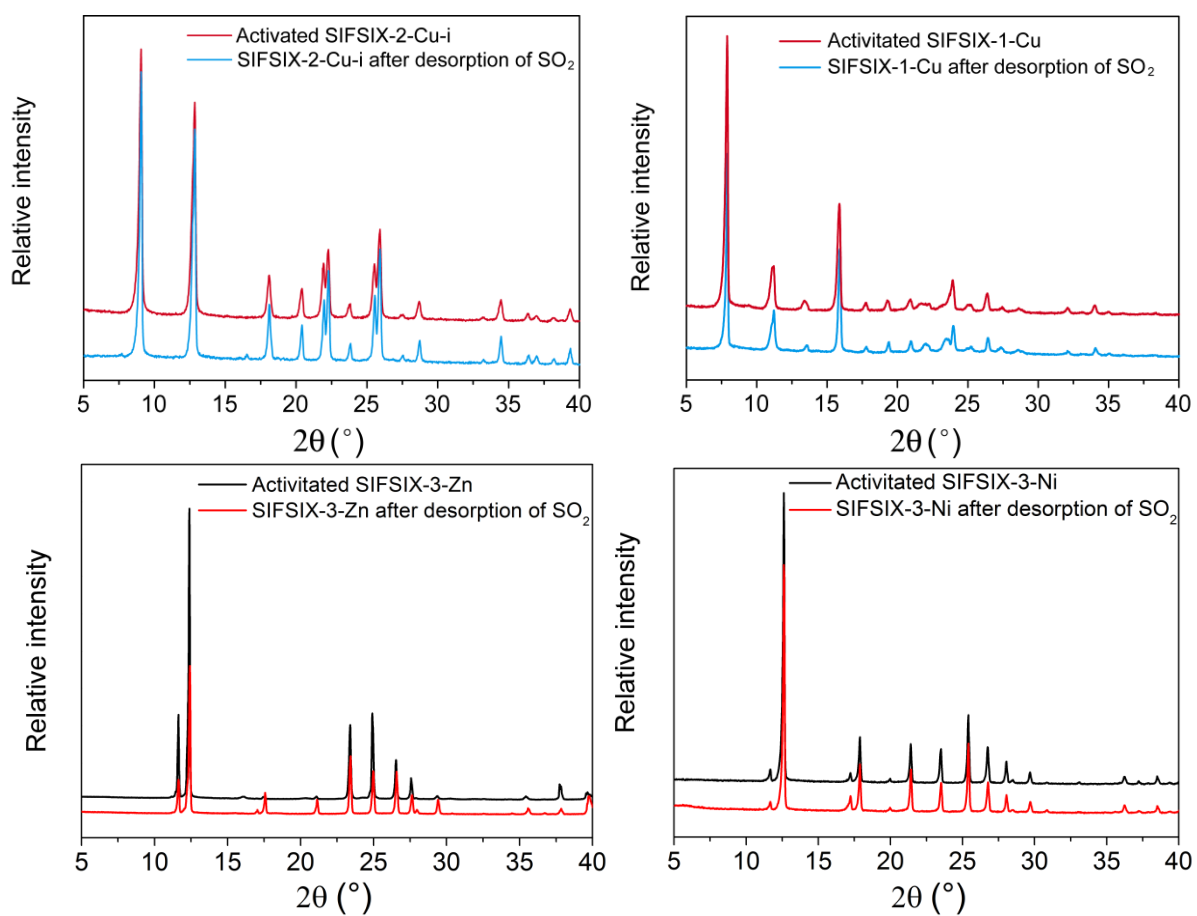


**Figure S6.** PXRD patterns of sample SIFSIX-2-Cu-i (A), SIFSIX-1-Cu (B), SIFSIX-3-Zn (C) and SIFSIX-3-Ni (D).

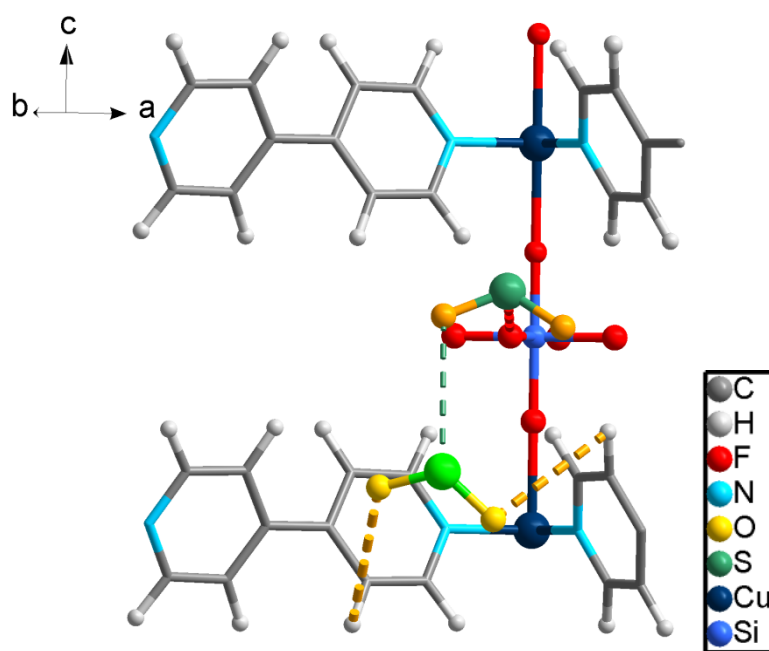


**Figure S7** Schematic pictures from DFT-D simulation reveal the SO<sub>2</sub> adsorbed at the secondary adsorption sites of SIFSIX-1-Cu through dipole-dipole interactions. (Note: the secondary adsorbed SO<sub>2</sub> molecules were highlighted with bright colour).



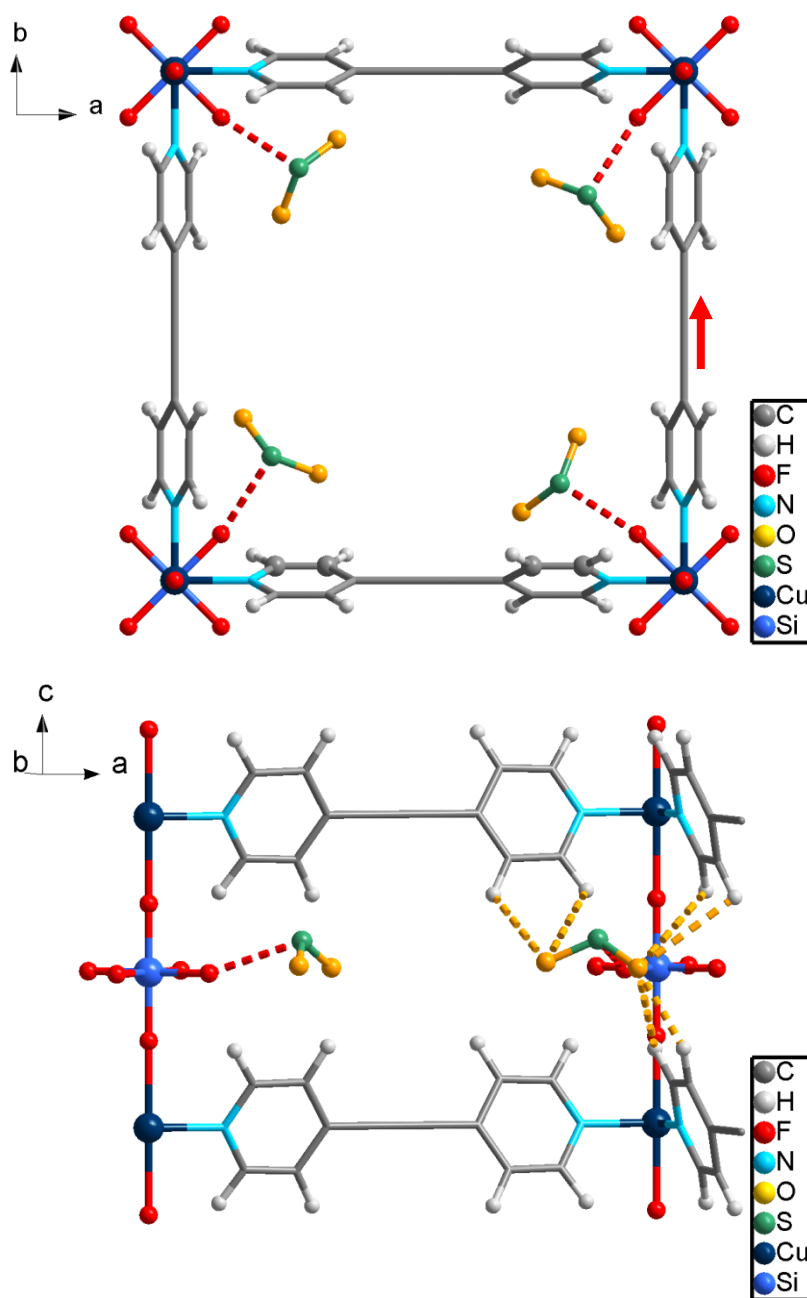


**Figure S8** DFT-D simulated optimized SO<sub>2</sub> adsorption sites of SIFSIX-2-Cu in two different viewing directions (A and B).

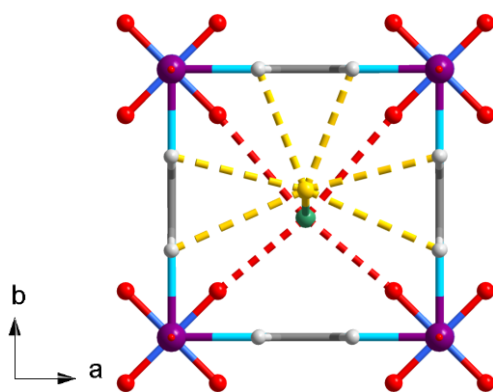


**Figure S9** DFT-D simulated optimized SO<sub>2</sub> adsorption sites of SIFSIX-3-Zn viewed down the *c* axis.

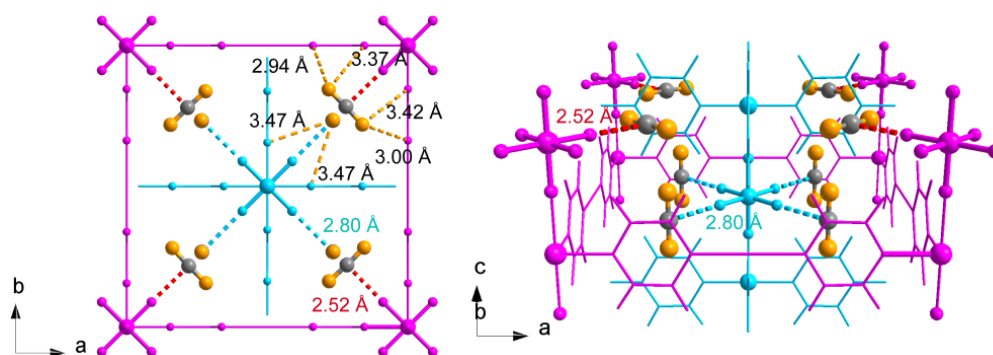


**Figure S10.** DFT-D calculated  $\text{CO}_2$  adsorption sites in SIFISX-2-Cu-i viewing in two different directions (A and B). (Note: the different nets are highlighted in magenta and cyan for clarity).

As shown in Figure S10,  $\text{CO}_2$  were trapped in the interpenetrated SIFISX-2-Cu-i through  $\text{C}^{\delta+} \cdots \text{F}^{\delta-}$  and multiple  $\text{O}^{\delta-} \cdots \text{H}^{\delta+}$  interactions. The DFT-D calculated distance of  $\text{C} \cdots \text{F}$  from different nets are 2.80 and 2.52 Å, respectively (Figure S10). By contrast, the DFT-D calculated distance of  $\text{S} \cdots \text{F}$  from different nets are both 2.44 Å, indicating much stronger electrostatic interactions between  $\text{SO}_2$  and SIFISX-2-Cu-i.

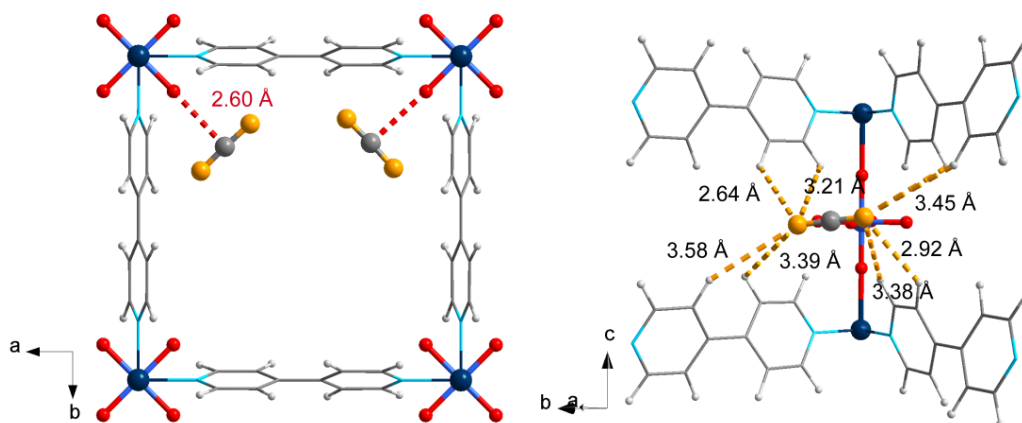


**Figure S11.** DFT-D calculated  $\text{CO}_2$  binding sites in SIFISIX-1-Cu viewing in two different directions (A and B). Colour code: F, red; Si, light blue; C, grey; H, light grey; N, sky blue; Cu, dark teal; O, orange.

In SIFISIX-1-Cu, the adsorbed  $\text{CO}_2$  are bound by the  $\text{C}^{\delta+} \cdots \text{F}^{\delta-}$  (Figure S11A) and multiple  $\text{O}^{\delta-} \cdots \text{H}^{\delta+}$  (Figure S11B) interactions. The DFT-D calculated distance of  $\text{C} \cdots \text{F}$  (2.60 Å) is comparable to the calculated distance of  $\text{S} \cdots \text{F}$  is 2.61 Å. And the DFT-D calculated  $\text{O} \cdots \text{H}$  distance of  $\text{CO}_2$  molecule with 4,4'-bipyridine ranged from 2.64 ~ 3.58 Å, longer than the  $\text{O} \cdots \text{H}$  distance of  $\text{SO}_2$  molecule with 4,4'-bipyridine (2.39~3.30 Å). These multiple interactions shows a stronger interactions between  $\text{SO}_2$  and SIFISIX-1-Cu.

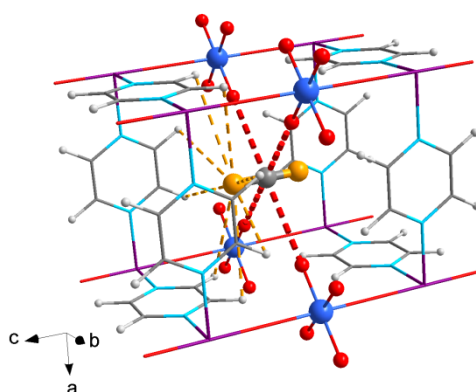


**Figure S12.** DFT-D calculated CO<sub>2</sub> binding sites in SIFSIX-3-Zn. Colour code: F, red; Si, light blue; C, grey; H, light grey; N, sky blue; Zn, violet; O, orange.

With a small pore size of SIFSIX-3-Zn, CO<sub>2</sub> were captured through four cooperative C<sup>δ+</sup>⋯F<sup>δ-</sup> and multiple O<sup>δ-</sup>⋯H<sup>δ+</sup> interactions. Adsorbed at the center of the one-dimensional channel (Figure S12), all of the four C⋯F distance were 3.36 Å.

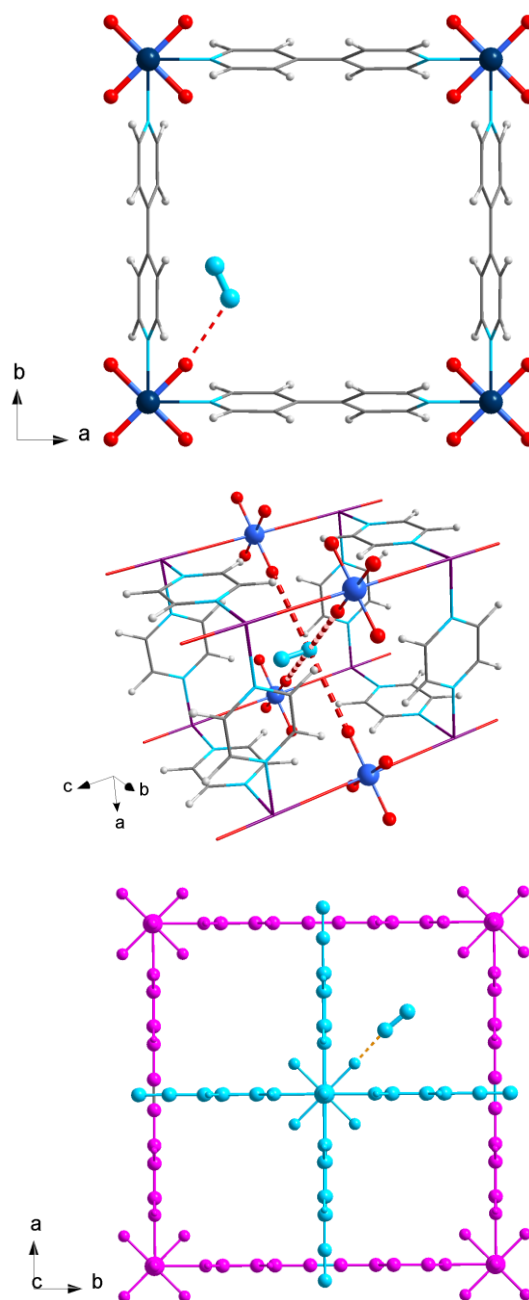


**Figure S13.** DFT-D calculated N<sub>2</sub> adsorption sites in SIFSIX-1-Cu (A), SIFSIX-3-Zn (B), and SIFSIX-2-Cu-i (C). Colour code: F, red; Si, light blue; C, grey; H, light grey; N, sky blue; Cu, dark teal; Zn, violet; O, orange. (Note: the different nets of SIFSIX-2-Cu-i are highlighted in magenta and cyan for clarity).

In addition, the calculated adsorption energy ( $\Delta E$ ) shows that there are much stronger interactions with SO<sub>2</sub> than CO<sub>2</sub> ( $\Delta E$  in SIFSIX-2-Cu-i, 50.2 versus 35.7 kJ mol<sup>-1</sup>;  $\Delta E$  in SIFSIX-1-Cu, 50.3 versus 31.1 kJ mol<sup>-1</sup>;  $\Delta E$  in SIFSIX-3-Zn, 54.1 versus 45.7 kJ mol<sup>-1</sup>). As for N<sub>2</sub>, the calculated  $\Delta E$  also shows that there are much stronger interactions with SO<sub>2</sub> than N<sub>2</sub> ( $\Delta E$  in SIFSIX-2-Cu-i, 50.2 versus 22.8 kJ mol<sup>-1</sup>;  $\Delta E$  in SIFSIX-1-Cu, 50.3 versus 15.7 kJ mol<sup>-1</sup>;  $\Delta E$  in SIFSIX-3-Zn, 54.1 versus 25.2 kJ mol<sup>-1</sup>).

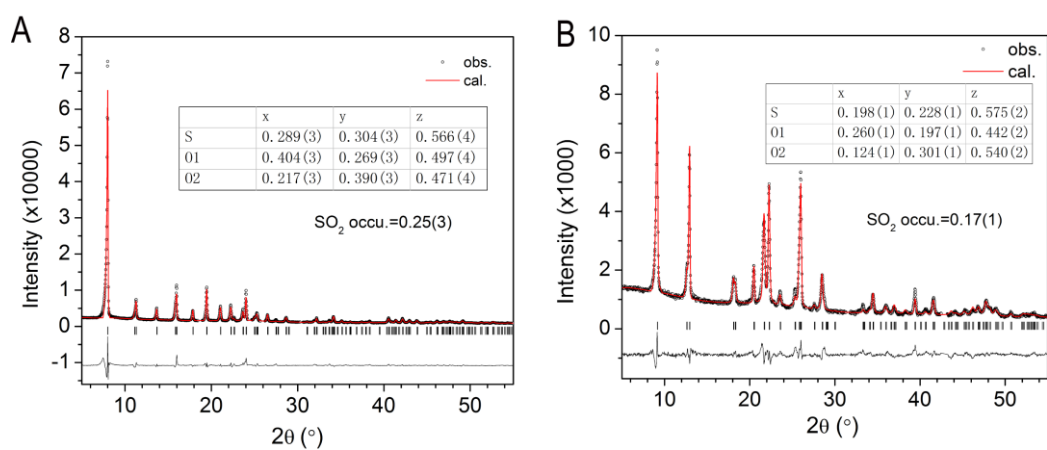


**Figure S14.** Powder X-ray diffraction patterns for the Rietveld refinement of SO<sub>2</sub>-loaded SIFSIX-1-Cu (A) and SO<sub>2</sub>-loaded SIFSIX-2-Cu-i (B). Goodness of fit data: (A)  $R_{wp} = 0.0891$ ,  $R_p = 0.0624$ ,  $\chi^2 = 3.96$ ; (B)  $R_{wp} = 0.0666$ ,  $R_p = 0.0492$ ,  $\chi^2 = 1.99$ .

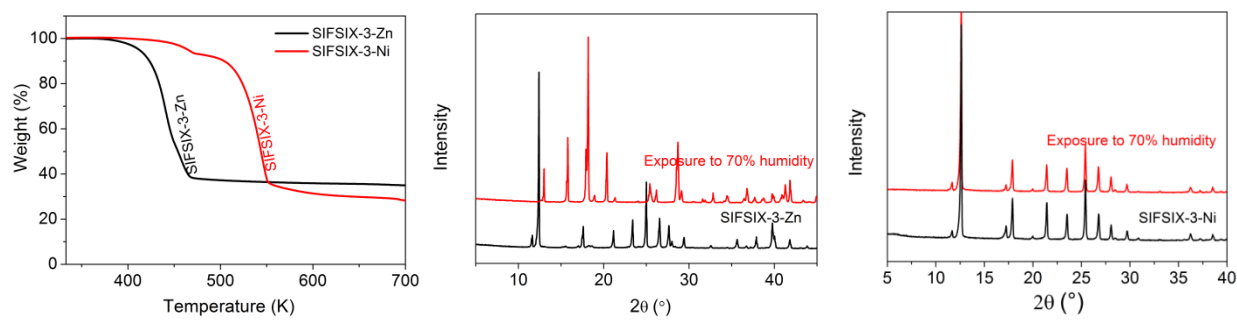


**Figure S15.** TGA patterns of sample SIFSIX-3-Zn and SIFSIX-3-Ni (A). XRD patterns of sample SIFSIX-3-Zn (B) and SIFSIX-3-Ni (C) after exposure to 75% humidity for 1 day.

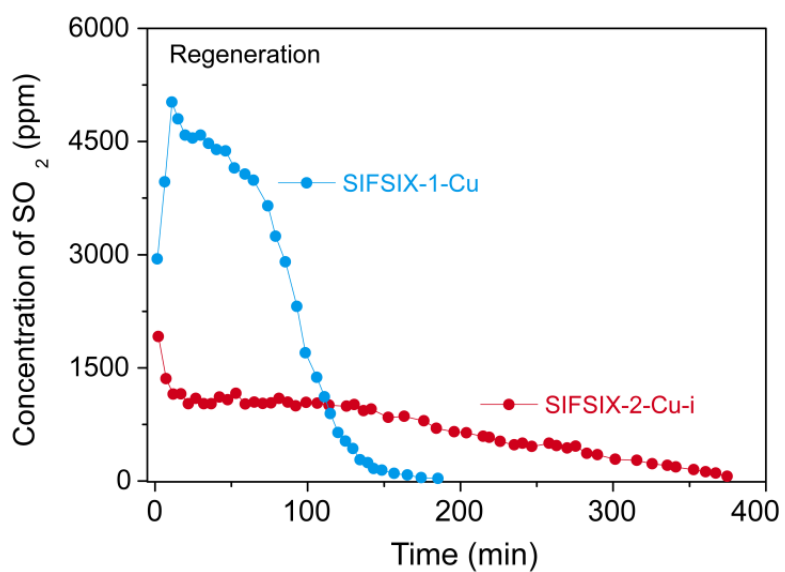


**Figure S16.** Experimental desorption curves for SO<sub>2</sub> on SIFSIX-2-Cu-i ( $\Phi 4.6 \times 50$  mm, 0.21 g) and SIFSIX-1-Cu ( $\Phi 4.6 \times 50$  mm, 0.23 g) with He flow of 20 ml min<sup>-1</sup> at 313 K.



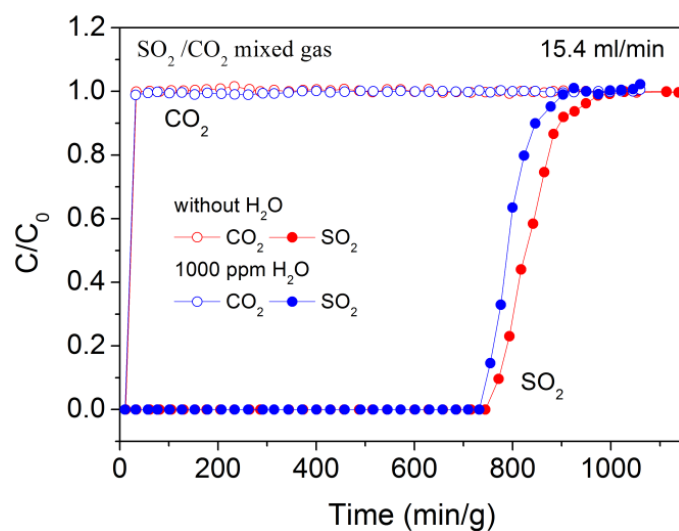


**Figure S17.** Experimental column breakthrough curves for SO<sub>2</sub>/CO<sub>2</sub> separations on SIFSIX-2-Cu-i (Φ4.6×50 mm, 0.21 g) at 298 K and 1.01 bar with the presence of moisture. The composition of the mixed gas: 1000 ppm H<sub>2</sub>O, 1870 ppm SO<sub>2</sub>, and 99.713% CO<sub>2</sub>.

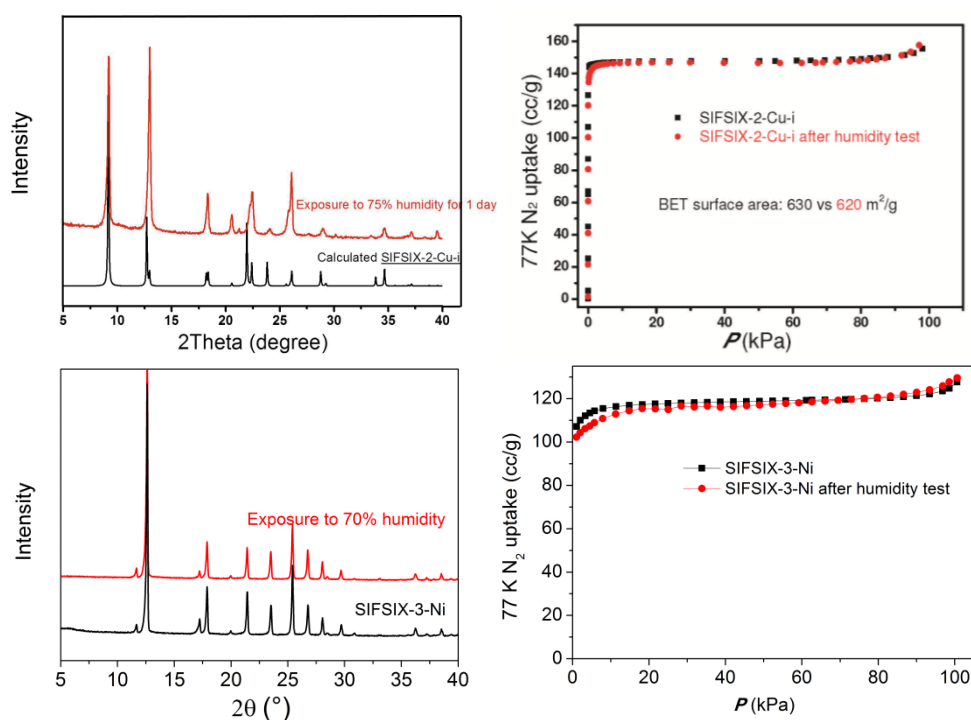


**Figure S18.** XRD patterns of sample SIFSIX-2-Cu-i after exposure to 75% humidity for 1 day (A). The BET curves of fresh SIFSIX-2-Cu-i and the sample after exposure to 75% humidity for 1 day (B). XRD patterns of sample SIFSIX-3-Ni after exposure to 70% humidity for 5 days (C). The BET curves of fresh SIFSIX-3-Ni and the sample after exposure to 70% humidity for 5 days (D).<sup>[6]</sup>

**Reference**

- [1] S.-I. Noro, R. Kitaura, M. Kondo, S. Kitagawa, T. Ishii, H. Matsuzaka, M. Yamashita, *J. Am. Chem. Soc.* **2002**, 124, 2569.
- [2] P. Nugent, Y. Belmabkhout, S. D. Burd, A. J. Cairns, R. Luebke, K. Forrest, T. Pham, S. Q. Ma, B. Space, L. Wojtas, M. Eddaoudi, M. J. Zaworotko, *Nature* **2013**, 495, 80.
- [3] A. Kumar, D. G. Madden, M. Lusi, K.-J. Chen, E. A. Daniels, T. Curtin, J. J. Perry IV, M. J. Zaworotko, *Angew. Chem. Int. Ed.* **2015**, 54, 14372.
- [4] X. Cui, K. Chen, H. Xing, Q. Yang, R. Krishna, Z. Bao, H. Wu, W. Zhou, X. Dong, Y. Han, B. Li, Q. Ren, M. J. Zaworotko, B. Chen, *Science* **2016**, 353, 141.
- [5] V. Barone, M. Casarin, D. Forrer, M. Pavone, M. Sambri, A. Vittadini, Role and effective treatment of dispersive forces in materials: polyethylene and graphite crystals as test cases, *Comput. Chem.* **2009**, 30, 934.
- [6] X. Cui, K. Chen, H. Xing, Q. Yang, R. Krishna, Z. Bao, H. Wu, W. Zhou, X. Dong, Y. Han, B. Li, Q. Ren, M. J. Zaworotko, B. Chen, *Science* **2016**, 353, 141.